

# The Disk and Extraplanar Regions of NGC 55

T. J. Davidge<sup>123</sup>

*Canadian Gemini Office, Herzberg Institute of Astrophysics,  
National Research Council of Canada, 5071 West Saanich Road,  
Victoria, B.C. Canada V9E 2E7*

tim.davidge@nrc.ca

## ABSTRACT

The stellar content of the nearby SB(s)m galaxy NGC 55 is investigated using images obtained with the Gemini South and Canada-France-Hawaii telescopes. The  $(K, H - K)$  and  $(K, J - K)$  color-magnitude diagrams (CMDs) of stars near the plane of the disk reveal signatures of large scale star formation during recent and intermediate epochs in the form of red supergiants (RSGs) with  $M_K \sim -11.5$ , and an asymptotic giant branch (AGB) that peaks near  $M_K = -10$ . Comparisons with stellar evolution models suggest that the brightest RSGs have an age near 8 Myr. A well-defined plume, which stellar evolution models suggest contains stars with masses near the RSG – AGB transition, is detected in CMDs constructed both from infrared and visible wavelength observations. It is concluded that star formation in the thin disk of NGC 55 has occurred at a significant rate for at least the past 0.1 – 0.2 Gyr, and this is consistent with other indicators. The near-infrared spectral-energy distribution (SED) of the integrated light near the center of the galaxy is consistent with that in other Magellanic irregular galaxies, indicating that the star-forming history of NGC 55, when averaged

---

<sup>1</sup>Based on observations obtained at the Gemini Observatory, which is operated by the Association of Universities for Research in Astronomy, Inc., under a co-operative agreement with the NSF on behalf of the Gemini partnership: the National Science Foundation (United States), the Particle Physics and Astronomy Research Council (United Kingdom), the National Research Council of Canada (Canada), CONICYT (Chile), the Australian Research Council (Australia), CNPq (Brazil), and CONICET (Argentina).

<sup>2</sup>Visiting Astronomer, Canada-France-Hawaii Telescope, which is operated by the National Research Council of Canada, the Centre National de la Recherche Scientifique, and the University of Hawaii.

<sup>3</sup>This publication makes use of data products from the Two Micron All Sky Survey, which is a joint project of the University of Massachusetts and the Infrared Processing and Analysis Center/California Institute of Technology, funded by the National Aeronautics and Space Administration and the National Science Foundation.

over timescales of 0.1 – 1 Gyr, has likely not been peculiar when compared with other late-type systems. Evidence is also presented that the disk contains a large population of old ( $\log(t_{yr}) \sim 10$ ) stars, and it is argued that a stable disk has been in place in NGC 55 for a significant fraction of the age of the Universe.

At projected distances in excess of 2 kpc off of the disk plane the brightest AGB stars have ages  $10_{-2}^{+3}$  Gyr. Thus, despite indications that dust and gas are present in the envelope surrounding the NGC 55 disk, the AGB content suggests that recently formed stars do not occur in large numbers in the extraplanar region. The  $(r' - i')$  colors of the RGB in the extraplanar region are consistent with  $[\text{Fe}/\text{H}]$  between  $-2.2$  and  $-0.7$ , with the majority of stars having  $[\text{Fe}/\text{H}] > -1.2$ , and the mean metallicity inferred from the RGB color does not change with distance above the disk plane. Thus, the stellar component in the extraplanar envelope is well mixed, at least in terms of metallicity. The mean metallicity of RGB stars is in excellent agreement with that measured in the extraplanar HII regions EHR 1 and 2, suggesting that the age-metallicity relation in this part of NGC 55 has been flat for at least a few Gyr. Finally, the RGB-tip occurs near  $i' = 23.1$  in the extraplanar region, and a distance modulus of 26.5 is computed from this feature.

*Subject headings:* galaxies:individual (NGC55) – galaxies: stellar content – galaxies: evolution – galaxies: distances and redshifts

## 1. INTRODUCTION

A current prevailing view is that large galaxies formed from the hierarchal accretion of smaller systems. In this picture, the first proto-galactic fragments were likely disks that had masses significantly smaller than the Milky-Way (Klypin et al. 1999), and obtained angular momentum from the torquing action of nearby mass concentrations. These early disks were consumed quickly in major mergers that kinematically heated the progenitors and induced large-scale star formation.

The merger activity that dominated during early epochs could have prevented the formation of stable, long-lived disks (e.g. Weil, Eke, & Efsthathiou 1998), and the epoch when stable disks appear in large numbers is of great importance for understanding the evolution of disk-dominated galaxies. Efforts to measure the age of the Galactic disk have yielded a range of results (e.g. discussion in Hansen 1999), and so studies of other galaxies are of great interest. Systems with disk-like light distributions are seen in large numbers at  $z > 2$  (e.g. Marleau & Simard 1998; Labbe et al. 2003), suggesting that they may be long-lived

structures even at high redshifts. Among nearby galaxies, an early epoch for the formation of stable disks is supported by the presence of metal-poor, and hence presumably old, globular clusters that appear to be associated with the thin disk of M31 (Morrison et al. 2004). The presence of such a cluster system in M31 may indicate that disks are relatively hardy entities, given the evidence for tidal interactions between M31 and its companions (Ferguson et al. 2002), which may have caused large-scale mixing (Brown et al. 2003; Bellazzini et al. 2003).

While long-lived disks may not form early-on, the extraplanar regions of spiral galaxies may contain stars with ages that span the time from the collapse of the first proto-galactic fragments to the epoch of disk formation and beyond. Efforts to simulate the formation of the Milky-Way predict that the halo started to form during early merging events that were tied to the creation of the bulge, and preceded the formation of the disk (e.g. Nakasato & Nomoto 2003; Bekki & Chiba 2001). A number of processes, such as the continued accretion of protogalactic material (Bekki & Chiba 2001), the disruption of satellites and the heating of the disk by tidal interactions (e.g. Sellwood, Nelson, & Tremaine 1998), as well as the ejection of gas outside of the disk plane by star forming events, which may cool so that stars can form (e.g. Savage et al. 2003), have the potential to add stars with a range of ages (and metallicities) to extraplanar environments.

Edge-on disk galaxies are important laboratories for investigating the evolutionary connections between halos, disks, and bulges. If halo and bulge formation are linked, then galaxies with very small bulges should have correspondingly small halos if compared with galaxies of similar size but earlier morphological type. On the other hand, if disk and halo formation are coupled then the relative sizes of halos and bulges should not be connected.

Dalcanton & Bernstein (2002) investigated the integrated photometric properties of undisturbed bulgeless edge-on disks, and found that they are embedded in diffuse flattened envelopes that show remarkable galaxy-to-galaxy similarities. The isophotes tend to become less flattened with increasing distance off of the disk, and the integrated photometric properties of the envelopes are consistent with an old population having an age in the range 6 – 8 Gyr. While there is a large range in the metallicities estimated for the envelopes, there are roughly equal numbers of systems with positive and negative metallicity gradients off the disk, and the mean trend is for metallicity not to change with height above the disk (e.g. Figure 10 of Dalcanton & Bernstein 2002). Given (1) the flattened nature of these envelopes and (2) that the target galaxies are bulgeless, Dalcanton & Bernstein (2002) associate the envelope with the disk, and argue that it is an artifact of merger activity that kinematically heated disk material.

The nearby collection of galaxies in Sculptor is one of the closest ensembles of galaxies

outside of the Local Group. The galaxies that are traditionally associated with this group extend over at least 1.5 Mpc along the line of sight, and may not form a gravitationally bound system (e.g. Karachentsev et al. 2003). The brightest members are late-type galaxies, and so the Sculptor group is an important laboratory for studying disk-dominated systems.

One of the closest members of the Sculptor group is NGC 55. This galaxy is inclined at an angle near  $81^\circ$  (Kiszkurno-Koziej 1988), and so is favourably oriented to study the extraplanar region. However, the near edge-on orientation also complicates efforts to study the morphology of NGC 55. Sandage & Tammann (1987) classify NGC 55 as an Sc galaxy. However, de Vaucouleurs (1961) concludes that NGC 55 is structurally similar to the LMC and that the main light concentration at visible wavelengths, which is offset from the geometric center of the galaxy, is a bar seen end-on. The SBm classification assigned by de Vaucouleurs (1961) is consistent with the HI properties of the galaxy, which were investigated by Hummel, Dettmar, & Wielebinski (1986), and who conclude that 20% of the mass is in the bar, while 80% is distributed throughout the disk. van den Bergh (2004, private communication) classifies NGC 55 as a dwarf irregular, and notes that a classification as early as Sc is unlikely given the absence of an obvious nucleus. For the current study it is assumed that NGC 55 is a Magellanic irregular.

Only a handful of studies have investigated the resolved stellar content of NGC 55. In a pioneering study Graham (1982) resolved red giant branch (RGB) stars off of the NGC 55 disk plane, demonstrating that a rich extraplanar population is present. Graham (1982) computed an upper limit of 26.4 to the distance modulus based on the peak red giant brightness. Pritchett et al. (1987) investigated the bright red stellar content near one end of the galaxy, and found that the luminosity function (LF) of asymptotic giant branch (AGB) stars is similar to that in other late-type galaxies. A population of C stars was identified, and Pritchett et al. (1987) computed a distance modulus of  $25.7 \pm 0.1$  based on the mean  $I$ -band magnitude of these objects. Davidge (1998) used infrared images to investigate the bright red stellar content in two NGC 55 disk fields. A prominent AGB sequence was detected, and the peak AGB brightness was found to be consistent with an age  $< 0.1$  Gyr. A population of red supergiants (RSGs) with  $K = 15$  was also found, from which Davidge (1998) computed a distance modulus of  $\mu = 26.0$ .

There is active star formation throughout much of the disk of NGC 55, and there are large quantities of gas off of the disk plane. Ferguson, Wyse, & Gallagher (1996) and Otte & Dettmar (1999) found shell structures and chimneys that are the signatures of supernovae explosions and stellar winds. Some of this gas has evidently cooled sufficiently to form stars, as Tüllmann et al. (2003) find two compact HII regions that are 2 – 3 arcmin ( $\sim 1 - 1.5$  kpc) off of the disk. If star formation has occurred for an extended period of time in this

region of NGC 55 then stars spanning a range of ages should be present in the extraplanar region.

In the current paper, the stellar contents of the disk and extraplanar regions of NGC 55 are investigated with the goal of providing insight into the past history of the galaxy. Two sets of observations are employed. One dataset, recorded with the CFHTIR imager on the 3.6 meter Canada-France-Hawaii Telescope (CFHT), consists of broad and narrow-band near-infrared images of a  $3 \times 7$  arcmin strip that slices through the center of NGC 55 and continues into the extraplanar region. The other dataset, obtained with GMOS on the 8 meter Gemini South (GS) telescope, consists of deep  $r'$  and  $i'$  images of a  $4.8 \times 4.8$  arcmin field that samples the extraplanar region and the outskirts of the star forming disk.

The paper is structured as follows. Details of the observations, the data reduction procedures, and the photometric measurements are presented in §2. The photometric properties of stars and star clusters near the disk plane are discussed in §3, while the photometric properties of extraplanar stars are examined in §4. A summary and discussion of the results follows in §5.

## 2. OBSERVATIONS & REDUCTIONS

### 2.1. CFHTIR Data

Three adjoining fields that form a north-south strip were imaged during the nights of November 21 - 23 2002 with the CFHTIR camera, which was mounted at the f/8 focus of the 3.6 metre CFHT. The detector in CFHTIR is a  $1024 \times 1024$  HgCdTe array. Each pixel subtends 0.21 arcsec on a side, and so the detector covers a  $3.6 \times 3.6$  arcmin<sup>2</sup> area.

A section of the DSS showing the area that was observed with the CFHTIR is shown in Figure 1. The entire strip was imaged through  $J$ ,  $H$ , and  $K'$  filters, with each of the three tiles being observed with a 4 point square dither pattern. Additional images of the southernmost tile, which samples the star-forming disk, were also recorded through narrow-band CO and  $K$  continuum filters. The total exposure time was 12 minutes per filter, with the exception of the observations through the CO filter, where the total exposure time was 24 minutes. The image quality in the processed images is  $\text{FWHM} = 1.0$  arcsec.

A series of dark frames were recorded at the end of each night. There was no measureable night-to-night variation in the dark count rate during the three night observing run, and so a master dark frame was constructed by combining darks recorded on all nights.

Flat-field frames were obtained at the beginning of each night. Images of a dome

spot were recorded with the flat-field lamps on and then off. The former frames contain information about pixel-to-pixel sensitivity variations and vignetting of the optical path that is required to flat-field the data, although thermal emission from uncooled objects along the optical path is also present. However, the latter frames contain information only about thermal emission from uncooled objects, and so a calibration image containing only flat-field information can be obtained by subtracting the images with lamps ‘off’ from those with lamps ‘on’. The flat field frames constructed in this manner showed no detectable night-to-night variations, and so a single master flat was created for each filter using flat-field data obtained throughout the run. Photometric studies of globular clusters, which are simple stellar systems and so are ideal for measuring uncertainties in the flat-field, using CFHTIR data indicate that the flat-field frames constructed in this manner track sensitivity variations across the field at roughly the 1% level.

A calibration frame that monitors signatures from thermal emission was constructed by median-combining flat-fielded images of ‘blank’ fields that were observed periodically throughout the run. Flat-fielded images of each sky field in each filter were corrected for DC sky variations, normalized to a common integration time, and then median-combined to reject sky sources.

The raw data were reduced using a standard pipeline for near-infrared imaging that corrects for additive (dark current, DC sky level, thermal emission, and interference fringes) and multiplicative (pixel-to-pixel sensitivity variations and vignetting of the optical path) effects using the calibration frames described above. The basic steps in the reduction process were: (1) dark subtraction, (2) the division by flat-field frames, (3) the subtraction of the DC sky level, which was measured on a frame-by-frame basis, and (4) the subtraction of the interference fringe and thermal emission calibration frame constructed for each filter. The individual processed images for each tile were spatially registered to correct for the dither offsets and then median-combined on a filter-by-filter basis. The combined images were trimmed to the region of common overlap, and the final  $K'$  image of the southernmost tile is shown in Figure 2.

## 2.2. GMOS Data

Broad-band  $r'$  and  $i'$  images of a field to the south of NGC 55, the location of which is indicated in Figure 1, were recorded with the GMOS imaging spectrograph on GS during the nights of October 18 and 21, 2003. The detector mosaic in GMOS consists of three  $2048 \times 4068$  EEV CCDs, with each pixel sampling 0.072 arcsec on a side. The detector was binned  $2 \times 2$  during readout for these observations, and so the angular scale is 0.144 arcsec

superpixel<sup>-1</sup>. Crampton et al. (2000) describe the various GMOS components in detail.

Six 150 sec exposures, recorded with a  $2 \times 3$  point dither pattern to allow the gaps between the detector elements to be filled during processing, were obtained in each filter. A control field, located midway between NGC 55 and NGC 247 with  $\alpha = 00^{\text{hr}}31^{\text{min}}58.1^{\text{sec}}$  and  $\delta = -29^{\circ}54'57.8''$  (E2000), was also observed with a total exposure time of 2700 sec per filter. This longer exposure time for the control field was needed to match observations of a field in the halo of NGC 247, which is the subject of a separate paper (Davidge 2004, in preparation). The image quality in the NGC 55 and control field images is roughly 0.6 arcsec FWHM.

Bias frames were recorded at various times throughout the two week observing run, and these were median-combined to create a master bias frame. Flat-field frames were constructed from unguided images of the twilight sky. Each twilight sky image was normalized to produce a mean flux level of unity, and the results were median-combined to suppress objects on the sky. The results track pixel-to-pixel sensitivity variations and vignetting across the science field at better than the 1% level. Finally, an  $i'$  fringe frame was constructed by median-combining individual images of the NGC 55 and control field frames. The fringes are suppressed at a level that is less than 1% of their original amplitude. Interference fringes are not evident in the  $r'$  data, and so a fringe frame was not constructed for these data.

The data were reduced with a standard pipeline for CCD images that parallels in many respects the procedure described previously in §2.1 and utilizes the calibration frames discussed in the previous paragraph. The steps in the CCD reduction pipeline were: (1) the subtraction of the master bias frame, (2) the division by the flat-field frame, (3) the subtraction of the DC sky level from each exposure, and (4) for the  $i'$  data, the subtraction of the fringe frame. The individual exposures for each field were spatially registered to correct for dither offsets and then median combined. The combined images were trimmed to the area of common overlap, and the final  $r'$  images are shown in Figures 3 (NGC 55) and 4 (Control field).

### 2.3. Photometric Measurements and Analysis Strategy

The photometric measurements were made with the PSF-fitting program ALLSTAR (Stetson & Harris 1988). Tasks in DAOPHOT (Stetson 1987) were used to identify stars, measure preliminary brightnesses, and construct PSFs. The photometric calibration of the CFHTIR data was set using observations of standard stars from Hawarden et al. (2001), while for the GMOS data this was done using standard stars from Landolt (1992). The

brightnesses and colors of the Landolt standards were transformed into the SDSS photometric system using equations from Fukugita et al. (1996). Based on the scatter in the standard star measurements, the photometric zeropoints have an uncertainty of a few tenths of a magnitude in  $J$ ,  $H$ , and  $K$  and less than 0.01 magnitudes in  $r'$  and  $i'$ .

Davidge (1998) discussed near-infrared photometry of a field in NGC 55 that was observed with the CIRIM camera on the CTIO 1.5 meter telescope and that overlaps the southern end of the CFHTIR strip. Although there is a significant difference in angular resolution between the two datasets (FWHM = 1.5 – 1.8 arcsec for the CTIO data, compared with 1.0 arcsec for the CFHT data), the photometric measurements of the stars with  $K < 16$  made with the two instruments are in reasonable agreement. In particular, the mean difference in  $K$ , in the sense CFHTIR – CIRIM, is  $\overline{\Delta K} = 0.18 \pm 0.13$ , while for  $J - K$  it is  $\overline{\Delta(J - K)} = -0.05 \pm 0.06$ . The quoted errors are the standard deviations about the mean. Crowding is more of an issue for stars in the CTIO images given the poorer angular resolution, and this will bias upwards brightnesses obtained from these data, which is consistent with the sign of  $\overline{\Delta K}$ .

Completeness fractions and the random errors in the photometry were assessed by running artificial star experiments. Based on the CMDs constructed from the data and discussed in §3 and 4, artificial stars inserted into the CFHTIR data were assigned colors matching those of AGB stars, while artificial stars inserted into the GMOS data had colors appropriate for RGB stars. Artificial stars were considered to be recovered only if they were detected in two or more filters. These experiments indicate that the 50% completeness level occurs at  $K = 18$  in the densely populated regions near the NGC 55 disk plane, and  $K = 19.5$  in the less crowded extraplanar regions. As for the GMOS data, the 50% completeness level occurs near  $i' = 25.5$  in the extraplanar regions.

If two or more stars fall within the same angular resolution element then they will appear as a single object, and the artificial star experiments can be used to assess the incidence of such blends. Given the crowded nature of the NGC 55 disk almost all stars in the southernmost tile of the CFHTIR dataset are likely to be blends, but most of these involve a very faint star being combined with a bright object, so that the effect on the photometric properties of the brighter object are insignificant. However, if two sources having brightnesses within a few tenths of a magnitude of each other fall in the same resolution element then they will be detected as an object that is  $\sim 0.5$  mag brighter than the more luminous of the two progenitors. The artificial star experiments predict that in the disk of NGC 55 about 3% of detected objects with  $K = 17$  are blends of objects having comparable brightness, while by  $K = 18$  the blend fraction increases to 10%. These fractions drop considerably in the extraplanar regions. As for the GMOS data, blending only becomes significant near

the faint end, with 10% of the sources near  $i' = 25$  being blends of objects with comparable brightness.

The data discussed in this paper sample a range of environments. To facilitate the analysis and investigate the stellar contents of these environments, the galaxy was divided into the following regions: (1) the thin disk, which in turn was sub-divided into star clusters and the field, (2) the thick disk, and (3) a region that is loosely referred to as ‘the halo’. The boundaries of the various regions are marked in Figure 1, and the rationale for placing the boundaries shown in Figure 1 are discussed in the next paragraph.

There are two obvious star clusters in the CFHTIR data and the boundaries of these, indicated in Figure 2, were set by eye. Both of these clusters are sites of  $H\alpha$  emission in the map constructed by Tüllmann et al. (2003), and so are expected to be made up of young stars. The thin disk was defined to lie within two of the stellar disk vertical scale lengths measured by Kizskurno-Koziej (1988). Because NGC 55 is inclined slightly, the foreground and background portions of the disk broaden the projected width of the galaxy. Assuming a disk radius of 6 kpc, estimated from the POSS image, then a projected width of 2.2 arcmin on either side of the disk center line will include the thin disk regions of the near and far ends of the NGC 55 disk, and the thin disk boundaries shown in Figure 1 have this width. As for the thick disk, Dalcanton & Bernstein (2002) found that this component tends to extend to at least 5 vertical disk scale lengths off of the disk plane in very late-type disk systems. After accounting for the inclination of NGC 55 in the same way as was done for the thin disk, the thick disk boundaries were defined to fall between 2.2 and 4.4 arcmin off of the disk center line. Finally, the halo is defined simply as the region that falls beyond the outer boundary of the thick disk, although in §4 it is demonstrated that this region appears simply to be a low surface brightness extension of the thick disk. The stellar contents of the star clusters and thin disk field are discussed in §3, while the thick disk and halo regions are discussed in §4.

### 3. RESULTS: THE YOUNG DISK OF NGC 55

#### 3.1. The Thin Disk Field as Imaged with CFHTIR

The  $(K, H - K)$  and  $(K, J - K)$  CMDs of stars in the thin disk field are shown in the right hand panels of Figures 5 and 6. The  $(K, J - K)$  CMD in Figure 6 is in many respects similar to the CMDs of the NGC 55 fields studied by Davidge (1998), one of which overlaps with the area observed with the CFHTIR. In particular, the prominent vertical sequence in the Davidge (1998) CMDs have a peak  $K$ -band brightness and  $J - K$  color that matches

the CMD in the right hand panel of Figure 6. However, the CFHTIR CMD goes deeper and has less scatter than the Davidge (1998) CMDs, due to the larger aperture of the CFHT and better image quality.

The  $(K, J - K)$  and  $(K, H - K)$  CMDs both broaden towards the faint end. The standard deviation along the color axis for stars with  $K$  between 17.75 and 18.25 is  $\pm 0.26$  mag in  $H - K$  and  $\pm 0.36$  mag in  $J - K$ . For comparison, the artificial star experiments predict that random photometric errors introduce a scatter of  $\pm 0.09$  mag in  $H - K$  and  $\pm 0.15$  mag in  $J - K$  at  $K = 18$ . Given that the scatter in both CMDs exceeds the random photometric error predictions, it thus appears that the broadening of the CMDs near the faint end is due to a real spread in stellar content. Later in this section it is demonstrated that this spread is due to AGB stars having a range of ages.

The objects along the vertical sequence in the right hand panels of Figures 5 and 6 with  $K < 16.5$  are RSGs, while the sources on this sequence with  $K > 16.5$  are evolving on the AGB (see below). The nature of the stars in the thin disk field can be investigated further by examining their broad-band near-infrared spectral-energy distributions (SEDs). This is done in the upper panel of Figure 7, which shows the  $(J - H, H - K)$  two-color diagram (TCD) of stars in the thin disk with  $K < 17.5$ . The majority of stars have SEDs that are suggestive of M giants, although the SEDs of some are consistent with K and M dwarfs, indicating that they may be foreground objects. The stars with  $H - K > 0.4$  tend to scatter around the LMC LPV sequence, and there are some objects with  $J - K > 1.6$ , which is a color range dominated by C stars in the LMC (Hughes & Wood 1990).

The narrow-band CO and K continuum observations were used to measure the CO index of the brightest stars in the southernmost tile of the CFHTIR strip, and the  $(K, CO)$  CMD and  $(J - K, CO)$  TCD of stars in the thin disk field are shown in Figures 8 and 9. The stars fall along a single sequence in the CMD, and tend to have CO indices that are consistent with them being M giants, although some have CO indices that are indicative of RSGs. The brightest star in the thin disk field has a CO index near 0, suggesting that it may be a foreground dwarf.

The  $(M_K, J - K)$  CMD of the thin disk is shown in the right hand panel of Figure 10. A distance modulus of  $\mu_0 = 26.5$ , based on the RGB-tip brightness measured from the GMOS data (§4.2), has been adopted. Foreground reddening is negligible towards NGC 55 (Burstein & Heiles 1984), and so no reddening correction was applied. Also shown in Figure 10 are isochrones from Girardi et al. (2002). Given the overall similarities between NGC 55 and the LMC, a metallicity of  $Z = 0.008$  ( $[Fe/H] \sim -0.3$ ), which is comparable to the peak in the metallicity distribution function of giants in the LMC (Larsen, Clausen, & Storm 2000), might be appropriate for NGC 55. In fact, HII regions in NGC 55 have oxygen abundances

that are similar to those in the LMC, although NGC 55 may be deficient in nitrogen with respect to the LMC (Webster & Smith 1983). Tüllmann et al. (2003) argues that the typical disk metallicity of NGC 55 is  $Z = 0.007^{+0.002}_{-0.001}$ , based on the central HII region. Thus, the isochrones plotted in Figure 10 have  $Z = 0.008$ .

The  $\log(t) = 8.15$  isochrone is significant as it marks the onset of the AGB, and this isochrone comes close to matching the color of the AGB plume in NGC 55. The predicted peak AGB brightness also falls close to a discontinuity in the number counts along the vertical sequence in the CMD, although matching the AGB-tip brightness is problematic, as many bright AGB stars are photometric variables, with the brightest being observed near the peak of their light curves. The peak AGB brightness also has a slight metallicity sensitivity, such that  $M_K^{AGBT} = -9.8$  if  $Z = 0.008$ , which is 0.1 mag brighter than the predicted peak  $Z=0.004$  brightness. In any event, it appears that a significant number of AGB stars in the thin disk of NGC 55 have progenitor masses that are close to that needed for the AGB to form. These are accompanied by a sizeable population of fainter AGB stars with colors and brightnesses that are consistent with  $\log(t) \geq 9$ , indicating that this portion of NGC 55 has been an area of active star formation for at least the last 1 Gyr.

The comparison with the isochrones in Figure 10 indicate that stars with  $M_K < -10$  are RSGs, and it is evident that the RSG sequence in the thin disk extends to  $M_K = -11.5$ . This peak RSG brightness is roughly consistent with what is seen in other star-forming disk-dominated systems, although there is considerable galaxy-to-galaxy scatter. Late-type galaxies with integrated brightnesses comparable to NGC 55 have peak  $M_K$  stellar brightnesses between  $-11$  and  $-12$  (e.g. Rozanski & Rowan-Robinson 1994), while the brightest RSGs in the Magellanic Clouds have  $M_K < -11$  and  $J - K = 1$  (Elias, Frogel, & Humphreys 1985).

The age of the brightest RSGs can be estimated from their luminosities. The  $K$ -band bolometric correction for RSGs with  $J - K = 1$  is  $BC_K = 2.75$  (Elias et al. 1985), and so RSGs with  $M_K = -11.5$  have  $M_{bol} = -8.7$ , or  $\log(L/L_\odot) = 5.4$ . This corresponds to stars with progenitor masses near  $25 M_\odot$ , or ages of  $\sim 8$  Myr based on the models computed by Fagotto et al. (1994). The bright RSGs are thus the result of very recent star formation throughout the disk of NGC 55.

The integrated near-infrared broad-band colors of the thin disk were measured to permit comparisons with other galaxies. There are prominent dust lanes in the area separating Clusters 1 and 2, and so the integrated colors were measured in a semi-circular annulus with a width of 10 arcsec that samples the disk to the north, south, and west of Cluster 1, but avoids the region between the two clusters. Caution must be exercised in making integrated photometric measurements of this nature, as the presence of a handful of very bright stars

may unduly influence aperture photometry. Therefore, rather than compute the mean flux in the area described above, the median flux was computed instead.

The location of the thin disk field on the TCD is shown in Figure 11, along with models for simple stellar systems from Leitherer et al. (1999). The location of the thin disk field on the TCD is appropriate for an intermediate-age system. This is not an unexpected result given the preponderance of AGB stars in the near-infrared CMDs of the thin disk field. The integrated colors of SB(s)m systems in the 2MASS Large Galaxy Atlas (Jarrett et al. 2003), as computed from the total brightness measurements, are also shown in Figure 11. The SB(s)m galaxies form a sequence that cuts diagonally across Figure 11, and the NGC 55 thin disk field falls along this sequence. This comparison indicates that the SED of the thin disk field, and thus the stellar content, is consistent with what is seen in other galaxies of similar morphological type.

### 3.2. The Thin Disk as Imaged with GMOS

The outer regions of the thin disk skirt the north east corner of the GMOS field, and the  $(i', r' - i')$  CMD of this portion of the GMOS dataset is shown in the left hand panel of Figure 12. The  $(i', r' - i')$  CMD of the corresponding region of the control field is shown in left hand panel of Figure 13. The control field contains a mixture of foreground stars and background galaxies, with the latter dominating near the bright end.

The GMOS data sample intrinsically fainter stars than the CFHTIR data because they were recorded with a much larger telescope and have better image quality. The  $(i', r' - i')$  CMD of the thin disk is dominated by RGB and AGB stars, with the RGB-tip near  $i' = 23.1$  (§4.2); the properties of the RGB in the thin disk are not discussed here because of the crowded nature of this part of the GMOS image, and a detailed discussion of the RGB in NGC 55 is deferred to §4.2. However, it is worth noting that the color of the RGB in the thin disk portion of the GMOS data is similar to what is seen in the thick disk, suggesting similar metallicities.

The  $(i', r' - i')$  CMD of the thin disk portion of the GMOS field is populated by stars spanning a range of ages, indicating that this portion of the thin disk has formed stars over an extended period of time. A population of blue stars with  $r' - i' = -0.3$  and  $i' > 21.5$  is present, and these likely belong to the youngest populations in this portion of NGC 55. Applying the transformation equations from Fukugita et al. (1996) indicates that the brightest blue stars have  $V \sim 21$ , or  $M_V \sim -5.5$ . These stars are thus near the bright end of the main sequence (e.g. Humphreys & McElroy 1984), and so may be very massive and

have ages consistent with, or even younger than, the RSGs discussed in §3.1 and 3.2.

There are two AGB sequences in the GMOS thin disk CMD. One sequence forms a plume with  $r' - i' \sim 0.4$  that extends roughly from the RGB-tip to  $i' = 21$ , while the other has  $i' > 22$ , and bends towards larger  $r' - i'$  colours, becoming difficult to track when  $r' - i' > 1.5$ . The nature of these AGB sequences is investigated in Figure 14, which shows the  $(M_{i'}, r' - i')$  CMD of the thin disk and the corresponding portion of the control field. A distance modulus of  $\mu_0 = 26.5$  has been assumed (§4.2). Also shown are  $Z=0.001$  and  $Z=0.008$  isochrones from Girardi et al. (2002), which were transformed into the SDSS filter system using relations from Fukugita et al. (1996).

The  $\log(t_{yr}) = 8.15$  isochrone roughly follows the vertical AGB plume. Given the number of objects in the control field CMD, it is likely that the bulk of stars with  $M_{i'} \sim -6$  are AGB stars in NGC 55, and not background or foreground contaminants. As for the fainter AGB sequence, while the  $\log(t_{yr}) = 10$  models with  $Z=0.001$  and  $Z=0.008$  have very different colors, it is clear that the upper envelope of the fainter AGB stars on the  $(M_{i'}, r' - i')$  CMDs is consistent with  $\log(t_{yr}) = 10.0$ . Therefore, the thin disk of NGC 55 contains stars that formed early in the life of the galaxy. Stars fall between the  $Z=0.008$   $\log(t_{yr}) = 8.15$  and  $10.0$  sequences, indicating that star formation continued during intermediate epochs.

The bolometric LF of AGB stars provides another means of probing the star-forming history of the thin disk of NGC 55. To construct such a LF from the GMOS data, AGB stars were selected based on (1) brightness, such that  $i' < 23.1$ , so as to be brighter than the RGB-tip, and (2) color, such that  $r' - i' > 0.2$  to avoid main sequence stars and include the blue edge of the AGB plume. While the thin disk of NGC 55 contains RSGs, these will have  $i' < 20$ , and no such objects are seen in the GMOS field.

Following Davidge (2003), the  $r' - i'$  colors and  $i'$  brightnesses were transformed into  $R - I$  and  $I$ , where  $R$  and  $I$  are in the Kron-Cousins system, using relations from Fukugita et al. (1996) and the relation between  $V - I$  and  $R - I$  for solar neighborhood giants from Bessell (1979). Bolometric magnitudes were then computed using  $I$ -band bolometric corrections for AGB stars from Bessell & Wood (1984). This procedure was also applied to objects in the thin disk portion of the control field, and the result was subtracted from the LF constructed from the NGC 55 thin disk field. The final bolometric AGB LF of the thin disk, corrected for objects in the control field, is shown in Figure 15.

The LF does not follow a single power-law, and there is a clear break near  $M_{bol} = -4.6$ . The majority of stars with  $M_{bol} > -4.6$  are on the AGB immediately above and to the right of the RGB-tip in the  $(i', r' - i')$  CMD. The location of these stars on the CMD is consistent with  $\log(t_{yr}) = 10$ , indicating that they have ‘old’ ages (see above). The break in the LF

thus suggests that the star formation rate in this region of the NGC 55 disk dropped at some point during the past  $\sim 10$  Gyr, and that a large fraction of the stars in the thin disk formed during early epochs.

Davidge (1998) investigated the bolometric LF of two areas in the disk of NGC 55, and it is of interest to see if a break occurs in those LFs near  $M_{bol} = -4.6$ . Unfortunately, after adjusting the LFs in Figure 11 of Davidge (1998) to the distance modulus adopted here, incompleteness becomes significant when  $M_{bol} > -5$ , and so these data do not go faint enough to determine if a break is present. Pritchett et al. (1987) also investigated the bolometric LF of AGB stars in NGC 55. After adjusting their LF to the distance modulus adopted here, the faint limit of the Pritchett et al. (1987) LF is  $M_{bol} \sim -5$ , and so these data also do not go faint enough to sample the discontinuity seen in the LF constructed from the GMOS data.

### 3.3. Clusters 1 and 2

The  $(K, H-K)$  and  $(K, J-K)$  CMDs of Clusters 1 and 2 are shown in the left hand and middle panels of Figures 5 and 6. The cluster CMDs show more scatter and are shallower than the thin disk CMDs, due to the higher stellar densities in the clusters. Indeed, Cluster 1 is more crowded than Cluster 2, and the CMDs of the former show a greater amount of scatter than the latter. It is likely that some of the stars in the cluster CMDs may be interlopers from the thin disk field. This being said, the brightest stars in the clusters are  $\sim 0.5$  mag in  $K$  fainter than in the thin disk field, and this leads to only a modest difference in age (see below).

The  $(J-H, H-K)$  TCD of stars with  $K < 17.5$  in both clusters is shown in the upper panel of Figure 7. As was the case in the thin disk, the majority of stars within the cluster boundaries have near-infrared SEDs that are similar to those of solar neighborhood M giants. There is considerable scatter among stars in both clusters with  $H-K > 0.3$ , which is the color interval occupied by LPVs in the LMC. Some stars in Cluster 1 fall in a region of the  $(J-H, H-K)$  TCD where  $J-K > 1.6$ , indicating that they may be C stars.

The  $(K, CO)$  CMDs of stars in Clusters 1 and 2 are shown in the left hand and middle panels of Figure 8, while the  $(J-K, CO)$  TCD of stars with  $K < 16$  in Clusters 1 and 2 is shown in the upper panel of Figure 9. The brightest stars in Clusters 1 and 2 define a relatively tight sequence in Figure 8, with  $\overline{CO} = 0.22$  when  $K < 16$ . The stars in Cluster 2 fall in a region of the  $(J-K, CO)$  TCD that is occupied by M giants, while many of the stars in Cluster 1 have CO indices that are consistent with them being RSGs. There is one star in

Cluster 1 with  $J - K \geq 1.5$  that has a CO index that is comparable to those of Milky-Way C stars. Finally, the brightest star in Cluster 2 has  $CO = 0.0$ , which is much weaker than the CO indices of the majority of stars in either cluster. Based on this weak CO index, it is likely that this object is a foreground star, and not a real member of the cluster.

The  $(M_K, J - K)$  CMDs of Clusters 1 and 2 are shown in the left hand and middle panels of Figure 10. The ideal means of measuring the age of Clusters 1 and 2 would be to use the brightness of the main sequence turn-off. While some bright blue stars are seen in the CMDs of both clusters near  $M_K = -9.5$ , there are not enough objects on which to base a reliable age determination, and these could be blue supergiants. Therefore, as with the thin disk field, the ages of Clusters 1 and 2 are estimated from the properties of the RSGs. The RSGs with  $M_K = -11$  have  $M_{bol} = -8.2$ , or  $\log(L/L_\odot) = 5.2$ . This corresponds to stars with progenitor masses near  $20 M_\odot$ , or an age of  $\sim 10$  Myr based on the Fagotto et al. (1994) models. Hence, although the brightest RSGs in the thin disk field are  $\sim 0.5$  mag brighter in  $K$  than their counterparts in Clusters 1 and 2, this leads to only a 2 Myr difference in age. The young age inferred for these clusters is consistent with them being sites of  $H\alpha$  emission (Tüllmann et al. 2003).

The integrated near-infrared photometric properties of Clusters 1 and 2 can be used to check the age estimated from the RSGs. Following the procedure described in §3.1 for the thin disk field, the integrated colors of the clusters were computed from median flux measurements to suppress the effects of individual bright stars. The background was measured in a 2 arcsec wide annulus immediately around each cluster.

The location of Clusters 1 and 2 on the  $(J - H, H - K)$  TCD is shown in Figure 11. A comparison with models from Leitherer et al. (1999) indicates that both clusters have near-infrared SEDs that are consistent with them being simple stellar systems with  $\log(t_{yr}) \sim 6.8$  and  $A_V$  between 1 and 2 magnitudes; thus, the integrated near-infrared colors of Cluster 1 and 2 are broadly consistent with the age inferred from the RSGs.

Davidge (2004) detected a population of young clusters near the center of the star-forming galaxy NGC 3077. The young NGC 3077 clusters discovered by Davidge (2004), which are also shown in Figure 11, form a relatively tight sequence on the TCD that roughly parallels the reddening vector. Clusters 1 and 2 have near-infrared SEDs that are similar to those of the NGC 3077 clusters, but with 1 – 2 magnitudes less extinction in  $V$ .

### 3.4. EHR 1

Tüllmann et al. (2003) discovered two star-forming regions that have projected distances of 1 – 1.5 kpc from the NGC 55 disk plane. One of these, EHR 1, falls within the boundaries of the thin disk region and was imaged with CFHTIR. Individual sources were not resolved in this object. However, the integrated brightness of EHR 1 in a 2.5 arcsec radius aperture is  $K = 16.1$ , with  $(H - K) = 0.72$  and  $(J - H) = 0.92$ . The near-infrared SED of EHR 1 is consistent with it being a very young system, and this is demonstrated in Figure 11, which shows the location of EHR 1 on the near-infrared TCD. EHR 1 falls on the NGC 3077 young cluster sequence in Figure 11, and a comparison with the Leitherer et al. (1999) models indicates that EHR 1 has an age of a few Myr, with  $A_V = 5 - 6$  magnitudes.

## 4. RESULTS: THE THICK DISK AND HALO

### 4.1. The CFHTIR Strip

The  $(K, H - K)$ , and  $(K, J - K)$  CMDs of the thick disk and halo portions of the CFHTIR strip are shown in Figures 16 and 17. There is a concentration of stars in the thick disk CMDs when  $K > 18.5$ , which is due to stars evolving on the AGB. In contrast, the CMDs of the halo region lack an obvious concentration of AGB stars.

The numbers of stars with  $K < 18$  in the thick disk and halo CMDs are similar, suggesting that the objects at this brightness likely do not belong to NGC 55. This is consistent with the near-infrared SEDs of these objects. The  $(J - H, H - K)$  TCD of stars with  $K < 17.5$  in the thick disk and halo is shown in the lower panel of Figure 7. While the majority of stars in the thin disk have near-infrared SEDs that are consistent with them being evolved giants, and hence are likely at the distance of NGC 55, many of the bright sources in the thick disk and halo regions fall systematically below the giant sequences on the TCD. In fact, the stars with  $H - K < 0.4$  occupy a portion of the TCD that suggests they are K and M main sequence stars, and so are likely foreground objects. Some of the brighter objects in the halo field have obvious extended morphologies, indicating that they are background galaxies.

The  $(M_K, J - K)$  CMDs of the thick disk and halo are shown in Figure 18. Based on the number of objects in each CMD, an excess population of stars in the thick disk with respect to the halo region only occurs when  $M_K > -7.5$ , and so  $M_K = -7.5$  is adopted as the AGB-tip brightness in the thick disk. The majority of resolved RGB stars in this portion of NGC 55 have metallicities between  $Z = 0.001$  and  $0.004$  (§4.2), and so the isochrones in Figure

18 have these metallicities. Given an AGB-tip brightness of  $M_K = -7.5$ , the isochrones in Figure 18 indicate that the resolved stars in the thick disk have an age that is close to  $\log(t_{yr}) = 10$ . The stellar contents of the thin disk and the thick disk thus appear to differ, in that the latter lacks the young and intermediate age populations seen in the former.

## 4.2. The GMOS Data

The  $(i', r' - i')$  CMDs of the thick disk and halo portions of the NGC 55 GMOS field are shown in the middle and right hand panels of Figure 12; the CMDs of the corresponding regions of the control field are shown in Figure 13. The number of objects with  $i' < 22$  in the control field is comparable to that in the thick disk and halo CMDs, indicating that many of the sources with  $i' < 22$  in the thick disk and halo are probably foreground and background objects. The bright main sequence stars and vertical AGB plume that were conspicuous in the thin disk are thus absent in detectable numbers, and this is consistent with what is seen in the CFHTIR data (§4.1).

Stars evolving on the RGB and AGB dominate the faint end of the thick disk and halo CMDs. The giant branch in the thick disk is much wider than predicted solely from photometric errors. Indeed, the standard deviation in  $r' - i'$  for stars with  $i'$  between 22.75 and 23.25 is  $\pm 0.12$  mag, whereas the artificial star experiments predict a scatter due to photometric errors of only  $\pm 0.03$  magnitudes. Thus, there is a real variation in stellar content among bright giants, and later in this section this is shown to be due to a spread in metallicity.

The brightness of the RGB-tip is a standard candle, and the RGB-tip brightness was measured from the thick disk data. The number counts in the thick disk CMD drop noticeably near  $i' = 23$ , indicating that the RGB-tip occurs close to this brightness. A better estimate of the RGB-tip brightness can be obtained from the  $i'$  LF of RGB stars in the thick disk, which is shown in Figure 19. The final LF was constructed by restricting the sample to objects with  $r' - i'$  between  $-0.5$  and  $1.5$  and then correcting for objects falling in the same color interval in the corresponding region of the control field.

The conventional means of measuring the brightness of the RGB-tip is to convolve the LF with a Stobel edge-detection kernel (e.g. Lee, Freedman, & Madore 1993). However, given the significant spray of AGB stars above the RGB-tip, it was decided to apply a different technique, which judges the position of the RGB-tip based on the departure from the power-law nature of the LF, as defined by RGB stars below the RGB-tip.

The NGC 55 LF shown in the lower panel of Figure 19 follows a power-law at the faint

end. A power-law was fit to the LF bins between  $i' = 23.5$  and  $25.0$ , which is an interval where the uncertainties in individual bins are modest and the artificial star experiments predict that incompleteness is not significant. A least squares fit to the thick disk LF entries in this brightness interval gives an exponent  $x = 0.22 \pm 0.01$ , which is within the range seen in globular clusters (e.g. Davidge 2000). The fitted power-law is compared with the data in the lower panel of Figure 19. The LF departs significantly from the fitted relation at  $i' \sim 23.1$ , and this is adopted as the brightness of the RGB-tip.

Lee et al. (1993) calibrated the RGB-tip as a standard candle in the I filter. Following Davidge et al. (2002), the relations computed by Fukugita et al. (1996) were used to transform the  $i'$  brightness of the RGB-tip into I, with the result that  $I^{RGBT} = 22.5$  for NGC 55. Adopting  $M_I^{RGBT} = -4$  (Lee et al. 1993), which holds for populations with  $[Fe/H] < -0.7$ , then the distance to NGC 55 computed from the RGB-tip is  $\mu = 26.5$ . No correction is applied for foreground extinction, as this appears to be small (Burstein & Heiles 1984).

With the distance to NGC 55 established from the brightness of the RGB-tip then the metallicity of the thick disk and halo can be estimated from the colors of RGB stars in the  $(i', r' - i')$  CMD. In Figure 20 the  $(M_{i'}, r' - i')$  CMD of RGB stars in the thick disk and halo are compared with  $\log(t_{yr}) = 10$  sequences from Girardi et al. (2002), transformed into the SDSS system using relations from Fukugita et al. (1996). The isochrones match the RGB-tip brightness and shape of the upper RGB in both the thick disk and halo regions. The majority of RGB stars in the thick disk appear to have a metallicity between  $Z = 0.001$  and  $Z = 0.003$ , although there are also stars that may be as metal-poor as  $Z = 0.0001$ . The RGB stars in the halo have a similar range of metallicities to those in the thick disk, and so there is no evidence for a metallicity gradient off of the disk plane.

There is a spray of objects above the RGB-tip in the thick disk CMD, and these are analogous to the AGB stars in the  $(K, J - K)$  CMD that were discussed in §4.1. The AGB stars in the left hand panel of Figure 20 are nicely bracketed by the  $\log(t_{yr}) = 10$  isochrones with  $Z=0.001$  and  $Z = 0.004$ ; in fact, the upper envelope of the AGB population in the left hand panel of Figure 20 is well matched by a line that connects the ends of the  $Z=0.001$  and  $Z=0.004$   $\log(t_{yr}) = 10.0$  AGB sequences. The inferred old age for the AGB stars is consistent with what was established from the CFHTIR data in §4.1.

What is the uncertainty in the age estimate determined from the comparisons in Figure 20? The age estimate is subject to uncertainties (1) in the models, (2) in the ability to locate the upper envelope of the AGB population on the CMD due to photometric variability, and (3) in the assumed distance to NGC 55. The uncertainties in the models are difficult to assess, and an error of  $\pm 0.1$  mag is (arbitrarily) assigned to this component. The scatter in the upper envelope of the thick disk AGB sequence on the CMD suggests that stellar

variability may contribute a  $\pm 0.1$  mag uncertainty. The errors in the distance estimates are more easily quantifiable, and are likely on the order of  $\pm 0.1$  mag, which is one half of the binning interval in Figure 19. If all three components are combined in quadrature then the total uncertainty in  $M_i^{AGBT}$  is  $\pm 0.2$  mag. The  $Z = 0.001$  AGB isochrones are more-or-less vertical in the  $(M_i, r' - i')$  CMD, and hence are well suited for assessing how an error in the AGB-tip brightness propagates into an uncertainty in the age estimate. The  $Z=0.001$  sequences from Girardi et al. (2002) indicate that a 0.2 mag change in  $M_i^{AGBT}$  translates into a 0.1 dex change in  $\log(t_{yr})$  near  $\log(t_{yr}) = 10$ , and so a  $\pm 0.1$  uncertainty is assigned to  $\log(t_{yr})$  estimated from the AGB-tip brightness. A lower limit to the age of the dominant stellar component in the envelope surrounding NGC 55 is thus 8 Gyr, while an upper limit is 13 Gyr.

While an AGB sequence is not seen above the RGB in the halo CMD, this does not mean that these stars are absent; rather, they may have a density that is sufficiently low to make their detection difficult. In fact, the  $i'$  LF of stars in the halo, corrected for sources in the control field, contains a modest population of stars that extend up to 0.6 mag in  $i'$  above the RGB-tip, indicating that AGB stars brighter than the RGB-tip do occur in this field. Based on the similar metallicities and age properties inferred from the CMDs, it appears that the halo and thick disk regions as defined here are not physically distinct entities; rather, they are part of the same structure.

Dalcanton & Bernstein (2002) find that the envelopes that surround their sample of undisturbed, bulgeless, edge-on disk galaxies have many properties in common. In particular, there is a distinct break between the main disk bodies and the surrounding envelopes, while the integrated colors of the thick disks indicate that the envelopes tend to have a metallicity that is comparable to the thin disk, and contain stars that formed  $\sim 6$  Gyr in the past. Finally, the envelopes also tend to be homogeneous stellar systems, in the sense that there is no evidence for age or metallicity gradients at moderately large distances off of the disk plane (e.g. Figure 10 of Dalcanton & Bernstein 2002).

While the properties of the envelope around NGC 55 are reminiscent of those in the Dalcanton & Bernstein (2002) sample, few envelopes in that sample have  $[\text{Fe}/\text{H}]$  as low as  $-1$ , and ages as old as 10 Gyr. The Dalcanton & Bernstein (2002) analysis relies on integrated photometric measurements, and so may be affected by the well known age-metallicity degeneracy. This degeneracy works in the sense that higher metallicities may be misinterpreted as older ages, with the result that if metallicity is overestimated then ages will be underestimated. Thus, if the metallicities of the envelopes in the Dalcanton & Bernstein (2002) sample were fixed at lower values then older ages would be predicted. This would then give results that are consistent with the NGC 55 envelope properties established here

from resolved stars.

## 5. DISCUSSION & SUMMARY

Moderately deep red and near-infrared images that were obtained with the CFHTIR imager on the CFHT and the GMOS imaging spectrograph on GS have been used to probe the stellar content of the nearby galaxy NGC 55. The data are used to investigate the stellar content along the disk plane and in the extraplanar region using evolved red stars as probes. The results of this investigation provide insight into the past history of the galaxy.

### 5.1. The Recent Star-Forming History of NGC 55

In §3.1 it was shown that the integrated near-infrared SED of the disk near the center of NGC 55 is similar to the SEDs of other Magellanic irregular galaxies, and is consistent with significant recent star formation. In fact, the thin disk field contains a population of RSGs that have brightnesses consistent with very young ages, indicating that the region near the center of NGC 55 has been the site of large scale star formation within the past 8 Myr. There are also two large clusters that have ages near 10 Myr. The CFHTIR data samples the disk near the main light concentration in NGC 55. The presence of very young stars in this portion of the NGC 55 disk may not be surprising if the main light concentration is a bar viewed end-on (de Vaucouleurs 1961), as the ends of bars in Magellanic-type galaxies tend to be sites of very recent star formation (Elmegreen & Elmegreen 1980).

A substrate of luminous AGB stars is seen throughout the thin disk, and comparisons with models from Girardi et al. (2002) indicate that these objects span a range of ages. A prominent feature in the CMDs constructed from both the CFHTIR and GMOS data is a plume that appears to contain stars with masses close to that needed to commence evolution on the AGB. A plume of stars with a similar color and peak brightness is seen in the CMDs of the two NGC 55 fields studied by Davidge (1998). One of the Davidge (1998) fields samples a region of the NGC 55 disk that is, like the regions observed with GMOS, well offset from the optical center of the galaxy. Thus, the stars on the AGB plume occur throughout the disk of NGC 55.

The detection of large numbers of stars with masses near the RSG – AGB evolutionary transition provides clues into the star-forming history of NGC 55 during recent epochs. One possibility is that NGC 55 is being viewed at a fortuitous time following an isolated episode of star formation when the RSG – AGB transition just happens to be occurring. However, it

is more likely that the detection of significant numbers of stars with masses close to those needed to evolve on the AGB indicates that there has been vigorous star formation during the past 0.1 – 0.2 Gyr. In fact, data from other sources indicate that the SFR in NGC 55 during the past 0.1 - 1 Gyr has been at least as high as that at the present day, and that it is more likely that the star formation rate (SFR) of NGC 55 has recently dropped. A number of indicators support a present-day SFR of at most a few tenths of a  $M_{\odot} \text{ year}^{-1}$ . The FIR luminosity and radio continuum emission from NGC 55 suggest that the present-day SFR is  $0.3 M_{\odot} \text{ year}^{-1}$  (Dettmar & Heithausen 1989), while the integrated  $H\alpha$  flux of NGC 55 is consistent with a SFR of  $0.16 M_{\odot} \text{ year}^{-1}$  (Ferguson et al. 1996). The SFR computed from x-ray flux measurements ranges between  $0.06$  and  $0.18 M_{\odot} \text{ year}^{-1}$ , based on equations 14 and 15 of Ranali, Comastri, & Setti (2003). Recent FIR flux measurements from the Spitzer Space Telescope yield a SFR of  $0.22 M_{\odot} \text{ year}^{-1}$  (Engelbracht et al. 2004). These various estimates of the present-day SFR are significantly lower than what is computed from the blue luminosity, which is a measure of the SFR averaged over the past Gyr, and which predicts a SFR of  $1.6 M_{\odot} \text{ year}^{-1}$  in NGC 55 (Dettmar & Heithausen 1989). Further evidence that the SFR has dropped during the past  $60 \times 10^7$  years comes from the high SNe rate needed to explain the extended x-ray emission around the galaxy (Oshima et al. 2003). There may have been brief lulls in star-forming activity, as Tüllmann et al. (2003) argue that breaks in the SFR may be needed to allow gas in the extraplanar region to cool sufficiently for stars to form, as has happened in EHR 1 and 2.

The stellar content throughout the thin disk of NGC 55 appears to be well mixed. For example, the distribution of the  $J - K$  colors of stars with  $K$  between 16.0 and 17.5 does not change with distance from the disk plane; a gradient in the color distribution would be expected if mean age changed with height above the disk plane. The ratio of objects with SEDs consistent with M giants to stars with SEDs similar to LMC LPVs also does not change with distance above the disk plane in the thin disk region. Adopting  $H - K = 0.3$  as the dividing line between M giants and LPVs in the TCD, then the ratio of M giants to LPVs is  $11/8 = 1.4 \pm 0.6$  in the portion of the thin disk between 1.1 and 2.2 arcmin from the disk plane, compared with  $162/125 = 1.3 \pm 0.2$  for stars within 1.1 arcmin of the disk plane.

The similarity in the stellar contents of the regions probed with the CFHTIR, which samples the disk plane, and GMOS, which samples the edge of the thin disk, further suggests that the disk of NGC 55 has experienced a remarkably uniform star-forming history. However, it should be kept in mind that NGC 55 is viewed nearly edge-on, and so any given site line samples stars from a large range in galactocentric distances. A high inclination can thus introduce an apparent uniformity in stellar content, as the star-forming history is smoothed over large portions of the galaxy. This also makes it easier to detect rare features in CMDs, such as the onset of the AGB, as the projected density of objects is higher than in other

orientations.

We close this portion of the discussion by noting that the contribution made by C stars to the total AGB luminosity peaks near  $\log(t_{yr}) \sim 8.7$  in moderately metal-poor systems (Maraston 1998); therefore, a large C star population might be expected in NGC 55 based on the star-forming history inferred from various sources, including the CFHT and GMOS data. However, Figure 9 of Pritchett et al. (1987) suggests that the C star frequency in NGC 55 may be relatively low given the integrated brightness of the galaxy. It is thus worth noting that candidate C stars with  $K < 17.5$  are seen in the  $(J - H, H - K)$  TCD of thin disk stars. These C stars may well be the tip of the iceberg, and their presence suggests that a rich C star population remains to be discovered in the disk of NGC 55.

## 5.2. The Extraplanar Region and the Early Evolution of NGC 55

The CFHTIR and GMOS data sample the extraplanar stellar content of NGC 55, and both datasets support an old age for this region of the galaxy; more specifically, based on the peak brightnesses of stars on the AGB there is no evidence for a young or intermediate age component outside of the region that is defined here as the thin disk. This result is perhaps surprising given the presence of gas and dust outside of the disk plane (e.g. Ferguson et al. 1996). Of course, the extraplanar region is not completely devoid of young stars, as there are some pockets of recent star formation (Tüllmann et al. 2003). Nevertheless, it appears that extraplanar star-forming regions like EHR 1 and EHR 2 have not contributed significantly to the stellar content of the envelope surrounding NGC 55.

The metallicities of EHR 1 and 2 suggest that they formed from material that did not originate in the thin disk (Tüllmann et al. 2003). In fact, the metallicities of these HII regions are in excellent agreement with the mean metallicity among RGB stars in the extraplanar region. This suggests that the age-metallicity relation in the extraplanar region may have been flat over a large fraction of the age of the Universe, after an initial period of rapid enrichment (see below). This could occur if the envelope has not been the site of large scale star formation for the past 10 Gyr or if it is unable to retain processed material. Another possibility is that there has been infall of metal-poor material at a rate that has fortuitously maintained the mean metallicity of the gas in the extraplanar region at a constant value.

The results of this study have implications for understanding the early evolution of NGC 55 in the context of the hierarchical formation model, although whether the envelope formed from the disruption of an early proto-disk or from the violent relaxation of proto-galactic gas clouds remains a matter of speculation. The absence of obvious metallicity gradients

indicates that the envelope formed in a highly coherent manner or has been well mixed since its formation. It is perhaps worth noting that the mean metallicity of the envelope around NGC 55 coincides with the point where the dynamical properties of the globular cluster system in the Milky-Way changes from orbits that are indicative of a pressure-supported system to one that has a significant rotational component (Zinn 1985), and this provides indirect evidence for a disk origin. Efforts to study the shape of the envelope will help constrain the origin of this structure. If the envelope originated from the disruption of a protodisk then it should not have a markedly flattened distribution.

The issue of how the envelope formed notwithstanding, that the RGB stars in the extraplanar region are old and typically have  $[\text{Fe}/\text{H}] \sim -1$  indicates that they likely formed from material that experienced rapid early enrichment. This is broadly consistent with the age-metallicity relation of the LMC during early epochs, which de Vaucouleurs (1961) argues is a galaxy that is structurally similar to NGC 55. The LMC age-metallicity relation climbs from  $[\text{Fe}/\text{H}] < -2$  to  $-1$  over a 3 Gyr period during early epochs (Hill et al. 2000), and an age dispersion of this size would affect the AGB-tip brightness in  $K$  in NGC 55 by only  $\sim 0.2$  mag (§4.2), making it difficult to detect. If the age-metallicity relations of NGC 55 and the LMC are similar then the absence of stars with  $[\text{Fe}/\text{H}] > -0.8$  would indicate that there should be no stars with ages less than  $\sim 10$  Gyr in the envelope around NGC 55, and this is consistent with the age inferred from the AGB-tip.

The chemical content of stars in the envelope around NGC 55 will provide additional clues into the origin of this structure. While there are as yet no abundance measurements of stars in the outer envelope of NGC 55, measurements of this nature have been made for metal-poor giants in the LMC, and the results are of interest in the context of the early evolution of Magellanic irregular galaxies. Hill et al. (2000) find that the metal-poor giants in the LMC fall along the trend between  $[\text{O}/\text{H}]$  and  $[\text{Fe}/\text{H}]$  defined by Galactic giants, suggesting that the metal-poor stars in the LMC may have formed in an environment similar to that from which the Galactic halo formed. However, the number of LMC giants in the Hill et al. (2000) sample is tiny, amounting to only four objects.

The globular cluster content of NGC 55 may present a problem for models in which the envelope around NGC 55 formed as the result of an early, violent collapse. If globular clusters form in supergiant molecular clouds (e.g. Harris & Pudritz 1994) that are associated with the major collapse events that are expected to produce rapid chemical enrichment, then a number of globular clusters might be expected in NGC 55 given the age and metallicity properties of stars in the envelope. Indeed, the LMC contains ten globular clusters with ages older than 10 Gyr (e.g. Geisler et al. 1997), and the majority of these are metal-poor, with  $[\text{Fe}/\text{H}] < -1$  (e.g. Hill et al. 2000). It appears that NGC 55 does not contain a large cluster

population, and may have a globular cluster content that differs from that of the LMC. Da Costa & Graham (1982) found three cluster candidates, one of which was identified as a young globular cluster, while Liller & Alcaïno (1983) found five candidate clusters. However, the nature of the clusters detected in these early surveys is in doubt, as Beasley & Sharples (2000) obtained spectra of a number of globular cluster candidates and concluded that the vast majority of these are background galaxies, with only one being a bona fide globular cluster.

The origin of the envelope around NGC 55 notwithstanding, the absence of a large population of young or intermediate age stars in the envelope indicates that the disk of NGC 55 has not been disrupted by major merger activity for a large fraction of the Hubble time; the conditions for a stable disk to form in this galaxy were evidently in place early on. In fact, NGC 55 is in a relatively isolated environment. It is one of four galaxies that are on the near side of the Sculptor group, and the largest member of this mini-group is NGC 300. The crossing time of this four galaxy ensemble is almost 19 Gyr (Karachentsev et al. 2003); consequently, the number of galaxy-to-galaxy interactions is expected to be small. Nevertheless, there are hints that NGC 55 may have been involved in recent interactions. The HI disk of NGC 55 is warped (Hummel et al. 1986), while NGC 55 is a barred galaxy, and bars are difficult to form without an external trigger, such as tidal interactions (e.g. Bottema 2003). This being said, the bar of the LMC contains a large population of stars with ages of at least a few Gyr (Ardeberg et al. 1997; Smecker-Hane et al. 2002), suggesting that the bars in Magellanic irregular galaxies can be long-lived, and so may not be indicative of recent interactions.

### 5.3. The Distance to NGC 55

The RGB-tip occurs near  $i' = 23.1$  in the thick disk of NGC 55, indicating that the distance modulus of this galaxy is 26.5. This distance measurement is likely not affected by dust internal to NGC 55, as the brightness of the RGB-tip does not change with distance off of the disk, and any dust will likely be concentrated close to the disk plane. The distance modulus of NGC 55 measured from the RGB-tip is larger than that computed previously from other indicators (§1). Nevertheless, given the distances to other nearby galaxies in this part of the sky (Karachentsev et al. 2003), the distance estimated from the RGB-tip still makes NGC 55 one of the nearest members of the Sculptor group.

Sincere thanks are extended to the anonymous referee, whose comments greatly improved the manuscript.

## REFERENCES

- Ardeberg, A., Gustafsson, B., Linde, P., & Nissen, P.-E. 1997, *A&A*, 322, L13
- Beasley, M. A., & Sharples, R. M. 2000, *MNRAS*, 311, 673
- Bekki, K., & Chiba, M. 2001, *ApJ*, 558, 666
- Bellazzini, M., Cacciari, C., Federici, L., Fusi Pecci, F., & Rich, M. 2003, *A&A*, 405, 867
- Bessell, M. S. 1979, *PASP*, 91, 589
- Bessell, M. S., & Brett, J. M. 1988, *PASP*, 100, 1134
- Bessell, M. S., & Wood, P. R. 1984, *PASP*, 96, 247
- Bottema, R. 2003, *MNRAS*, 344, 358
- Brown, T. M. et al. 2003, *ApJ*, 592, L17
- Burstein, D., & Heiles, C. 1984, *ApJS*, 54, 33
- Cohen, J. G., Frogel, J. A., Persson, S. E., & Elias, J. H. 1981, *ApJ*, 249, 481
- Crampton, D., et al. 2000, *SPIE*, 4008, 114
- Da Costa, G. S., & Graham, J. A. 1982, *ApJ*, 261, 70
- Dalcanton, J. J., & Bernstein, R. A. 2002, *AJ*, 124, 1328
- Davidge, T. J. 1998, *ApJ*, 497, 650
- Davidge, T. J. 2000, *AJ*, 120, 1853
- Davidge, T. J. 2003, *AJ*, 125, 3046
- Davidge, T. J. 2004, *AJ*, 127, 1460
- Davidge, T. J., Da Costa, G. S., Jorgensen, I., Allington-Smith, J. R. 2002, *AJ*, 124, 886
- Dettmar, R.-J., & Heithausen, A. 1989, *ApJ*, 344, L61
- de Vaucouleurs, G. 1961, *ApJ*, 133, 405
- Elias, J. H., Frogel, J. A., & Humphreys, R. M. 1985, *ApJS*, 57, 91
- Elmegreen, D. M., & Elmegreen, B. G. 1980, *AJ*, 85, 1325
- Engelbracht, C. W. et al. 2004, *ApJS*, 154, 248
- Fagotto, F., Bressan, A., Bertelli, G., & Chiosi, C. 1994, *A&AS*, 105, 29
- Ferguson, A. M. N., Wyse, R. F. G., & Gallagher, J. S. 1996, *AJ*, 112, 2567
- Ferguson, A. M. N., Irwin, M. J., Ibata, R. A., Lewis, G. F., & Tanvir, N. R. 2002, *AJ*, 124, 1452

- Frogel, J. A., Persson, S. E., Aaronson, M., & Matthews, K. 1978, *ApJ*, 220, 75
- Fukugita, M., Ichikawa, T., Gunn, J. E., Doi, M., Shimasku, K., & Schneider, D. P. 1996, *AJ*, 111, 1748
- Geisler, D., Bica, E., Dottori, H., Claria, J. J., Piatti, A. E., & Santos Jr., J. F. C. 1997, *AJ*, 114, 1920
- Girardi, L., Bertelli, G., Bressan, A., Chiosi, C., Groenewegen, M. A. T., Marigo, P., Salasnich, B., & Weiss, A. 2002, *A&A*, 391, 195
- Graham, J. A. 1982, *ApJ*, 252, 474
- Hansen, B. M. S. 1999, *ApJ*, 520, 680
- Harris, W. E., & Pudritz, R. E. 1994, *ApJ*, 429, 177
- Hawarden, T. G., Leggett, S. K., Letawsky, M. B., Ballantyne, D. R., & Casali, M. M. 2001, *MNRAS*, 325, 563
- Hill, V., Francois, P., Spite, M., Primas, F., & Spite, F. 2000, *A&A*, 364, L19
- Hughes, S. M. G., & Wood, P. R. 1990, *AJ*, 99, 784
- Hummel, E., Dettmar, R.-J., & Wielebinski, R. 1986, *A&A*, 166, 97
- Humphreys, R. M., & McElroy, D. B. 1984, *ApJ*, 284, 565
- Jarrett, T. H., Chester, T., Cutri, R., Schneider, S. E., & Huchra, J. P. 2003, *AJ*, 125, 525
- Karachentsev, I. D., et al. 2003, *A&A*, 404, 93
- Kiszkurno-Koziej, E. 1988, *A&A*, 196, 26
- Klypin, A., Kravtsov, A. V., Valenzuela, O., & Prada, F. 1999, *ApJ*, 522, 82
- Labbe, I. et al. 2003, *ApJ*, 591, L95
- Landolt, A. U. 1992, *AJ*, 104, 340
- Larsen, S. S., Clausen, J. V., & Storm, J. 2000, *A&A*, 364, 455
- Lee, M. G., Freedman, W. L., & Madore, B. F. 1993, *ApJ*, 417, 553
- Leitherer, C. et al. 1999, *ApJS*, 123, 3
- Liller, W., & Alcaïno, G. 1983, *ApJ*, 264, 53
- Maraston, C. 1998, *MNRAS*, 300, 872
- Marleau, F. R., & Simard, L. 1998, *ApJ*, 507, 585
- Morrison, H. L., Harding, P., Perrett, K., & Hurley-Keller, D. 2004, *ApJ*, 603, 87
- Nakasato, N., & Nomoto, K. 2003, *ApJ*, 588, 842

- Oshima, T., Mitsuda, K., Ota, N., & Yamasaki, N. Y. 2003 in Proceedings of the Workshop on Galaxies and Clusters of Galaxies, held at Shunzenji, October 2002, Japan Society for the Promotion of Science, p. 33
- Otte, B., & Dettmar, R.-J. 1999, *A&A*, 343, 705
- Pritchett, C. J., Richer, H. B., Schade, D., Crabtree, D., & Yee, H. K. C. 1987, *ApJ*, 323, 79
- Ranali, P., Comastri, A., & Setti, G. 2003, *A&A*, 399, 39
- Rozanski, R., & Rowan-Robinson, M. 1994, *MNRAS*, 271, 530
- Sandage, A., & Tammann, G. A. 1987, *A Revised Shapley-Ames Catalog of Bright Galaxies Second Edition* (Carnegie Institute: Washington)
- Savage, B. D. et al. 2003, *ApJS*, 146, 125
- Sellwood, J. A., Nelson, R. W., & Tremaine, S. 1998, *ApJ*, 506, 590
- Smecker-Hane, T. A., Cole, A. A., Gallagher, J. S. III, & Stetson, P. B. 2002, *ApJ*, 566, 239
- Stetson, P. B. 1987, *PASP*, 99, 191
- Stetson, P. B., & Harris, W. E. 1988, *AJ*, 96, 909
- Tüllmann, R., Rosa, M. R., Elwert, T., Bomans, D. J., Ferguson, A. M. N., & Dettmar, R.-J. 2003, *A&A*, 412, 69
- Webster, B. L., & Smith, M. G. 1983, *MNRAS*, 204, 743
- Weil, M. L., Eke, V. R., & Efsthathiou, G. 1998, *MNRAS*, 300, 773
- Zinn, R. 1985, *ApJ*, 293, 424

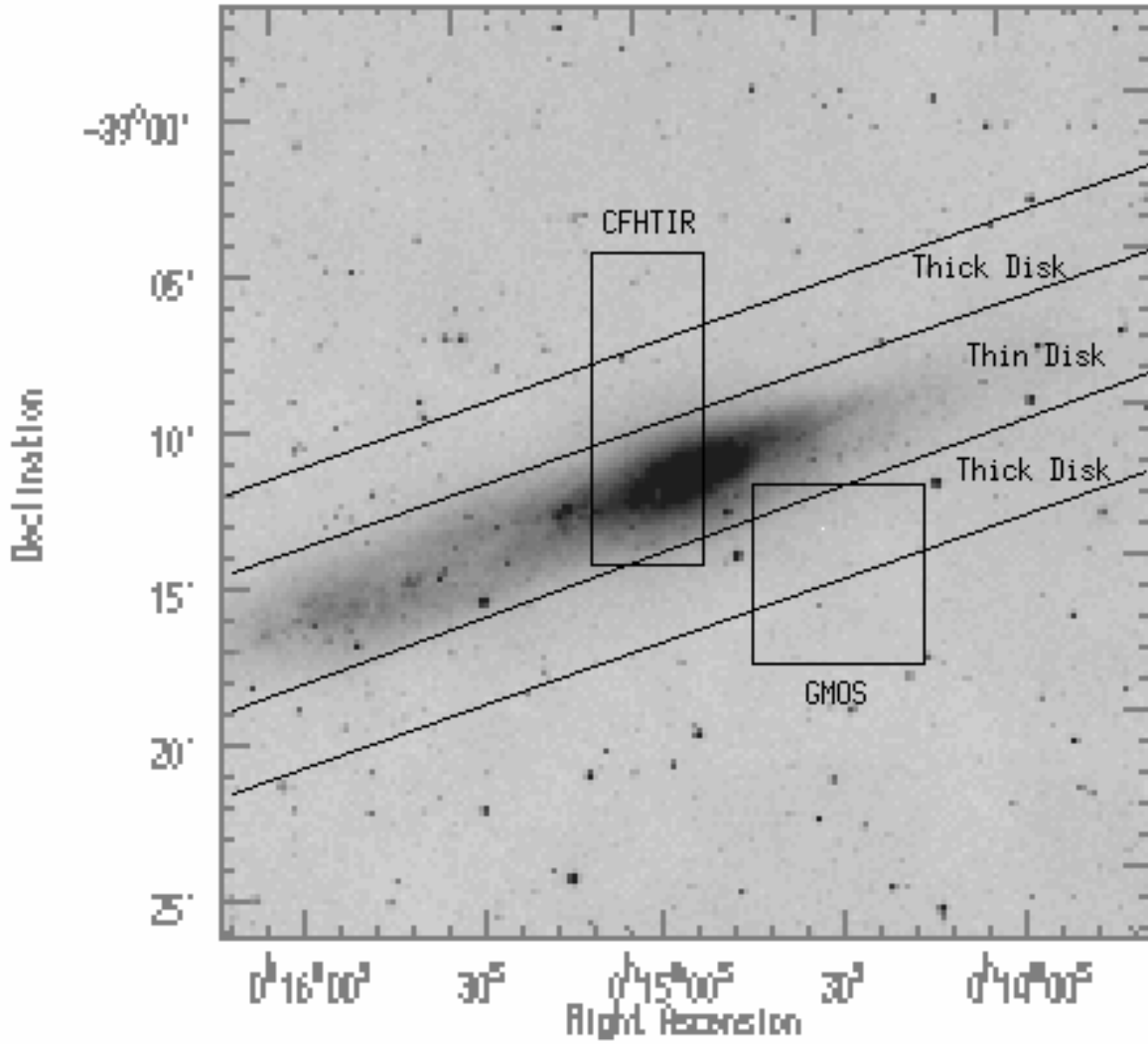


Fig. 1.— A  $30 \times 30$  arcmin section of the Digitized Sky Survey showing the areas imaged with the CFHTIR and GMOS. East is to the left, and North is at the top. The lines mark the boundaries of the thin disk, thick disk, and halo regions as defined in §2.3.

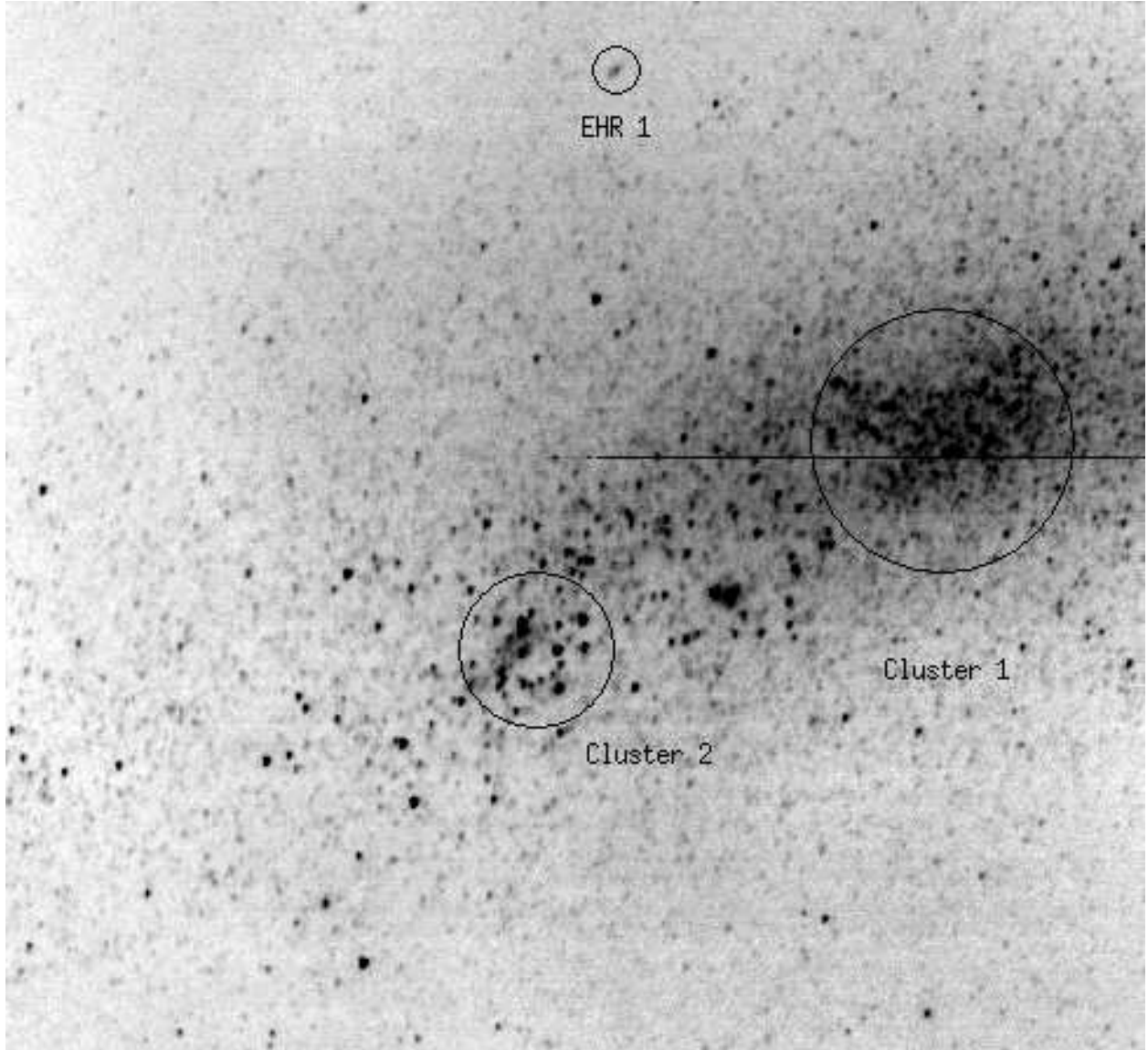


Fig. 2.— The final  $K'$  image of the southernmost tile in the CFHTIR mosaic. A  $3.6 \times 3.3$  arcmin field is shown. The two clusters that are discussed in §3 are indicated, as is the extraplanar HII region EHR 1. The horizontal line crossing through Cluster 1 is an artifact of the boundary between detector quadrants. East is to the left, and North is at the top.

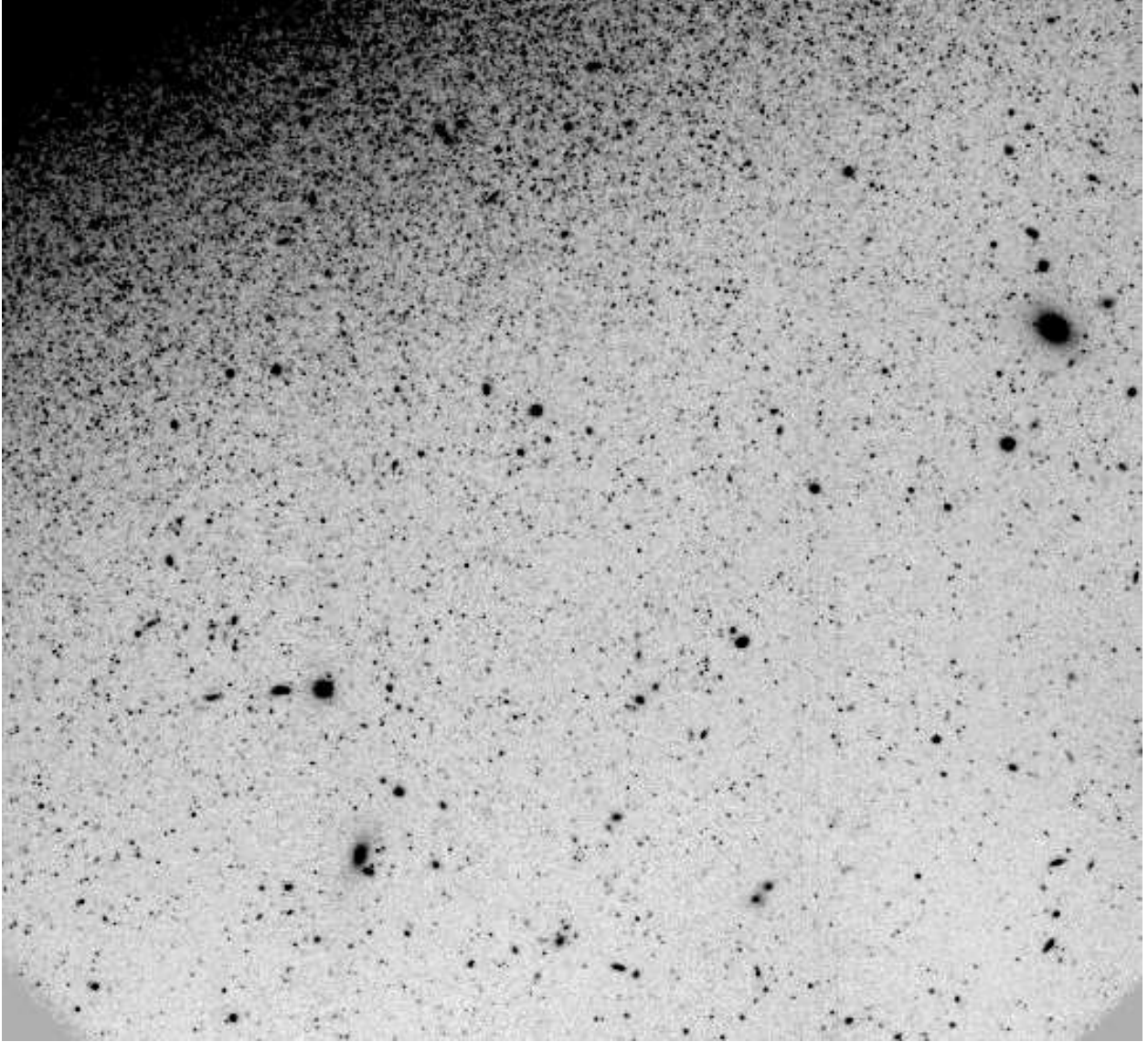


Fig. 3.— The final  $r'$  image of the NGC 55 GMOS field, which covers  $4.8 \times 4.8$  arcmin. The outer regions of the thin disk can be seen in the upper left hand corner. North is at the top, and East is to the left.

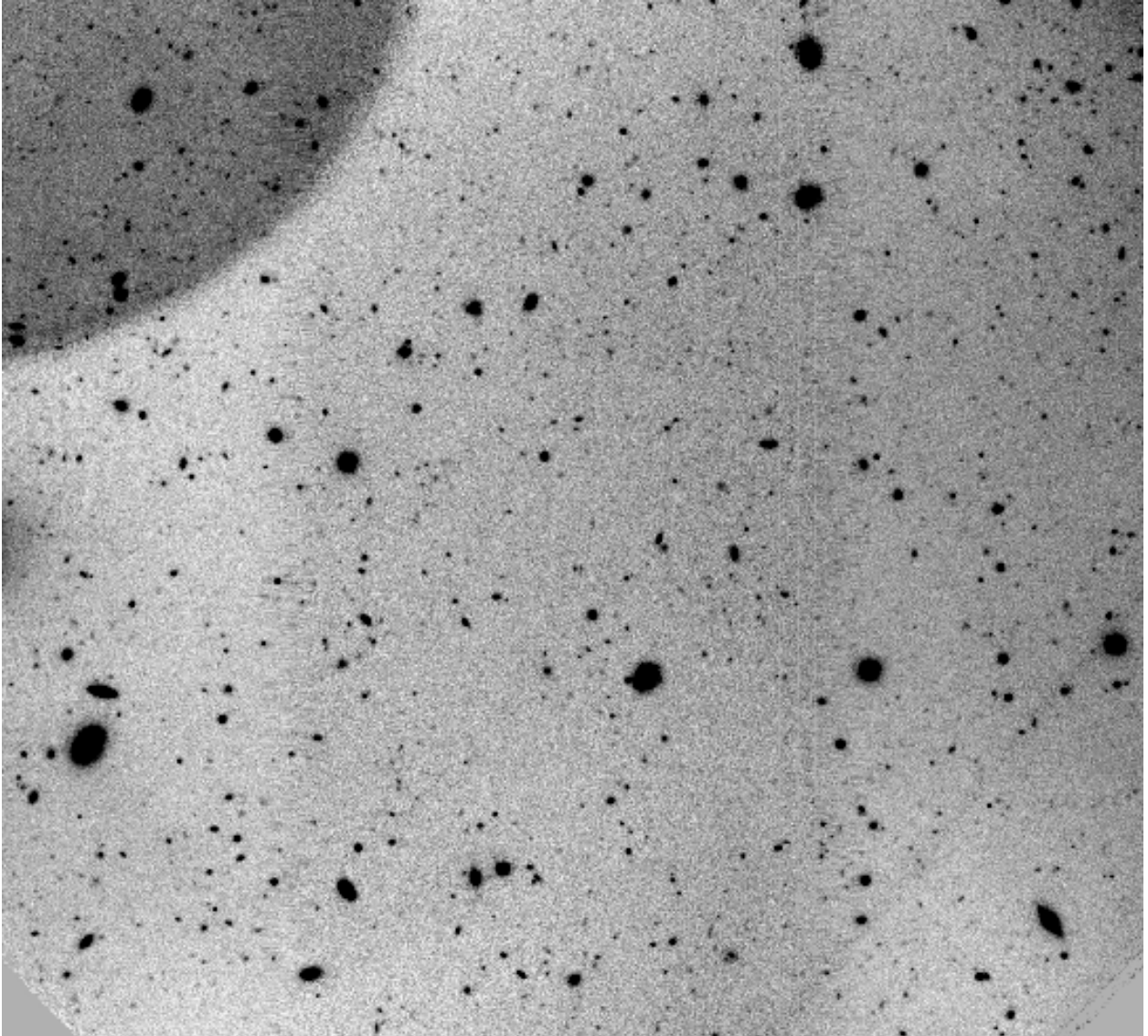


Fig. 4.— The final  $r'$  image of the GMOS control field, which covers  $4.8 \times 4.8$  arcmin. The slight brightening of the background sky level in the upper left hand corner is an artifact of a bright star that is off of the field. North is at the top, and East is to the left.

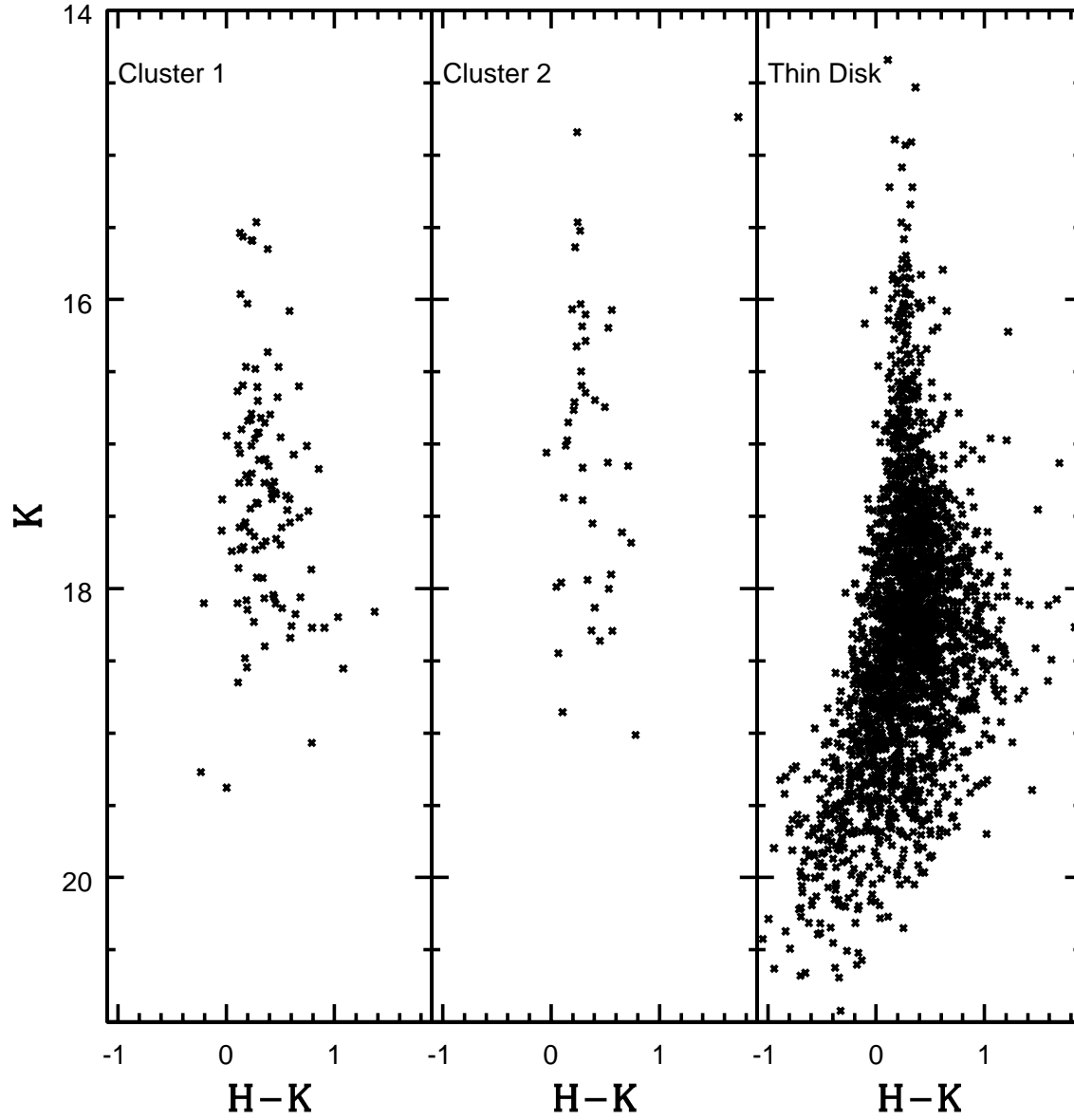


Fig. 5.— The  $(K, H - K)$  CMDs of Cluster 1, Cluster 2, and the thin disk field. The vertical sequence in each CMD is dominated by AGB stars when  $K > 16.5$  and RSGs when  $K < 16.5$ .

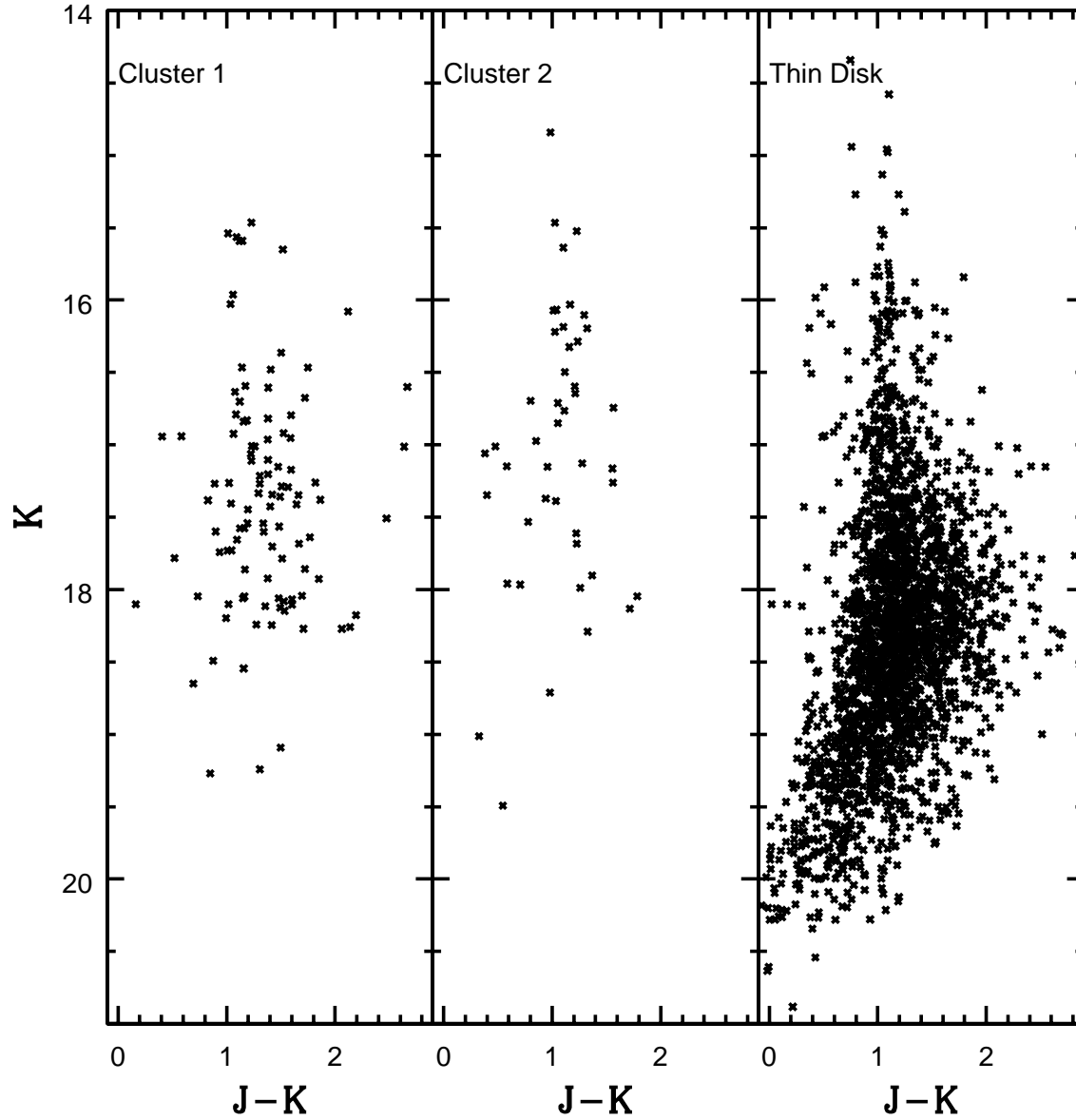


Fig. 6.— The  $(K, J - K)$  CMDs of Cluster 1, Cluster 2, and the thin disk field. The vertical sequence in each CMD is dominated by AGB stars when  $K > 16.5$ , and RSGs when  $K < 16.5$ .

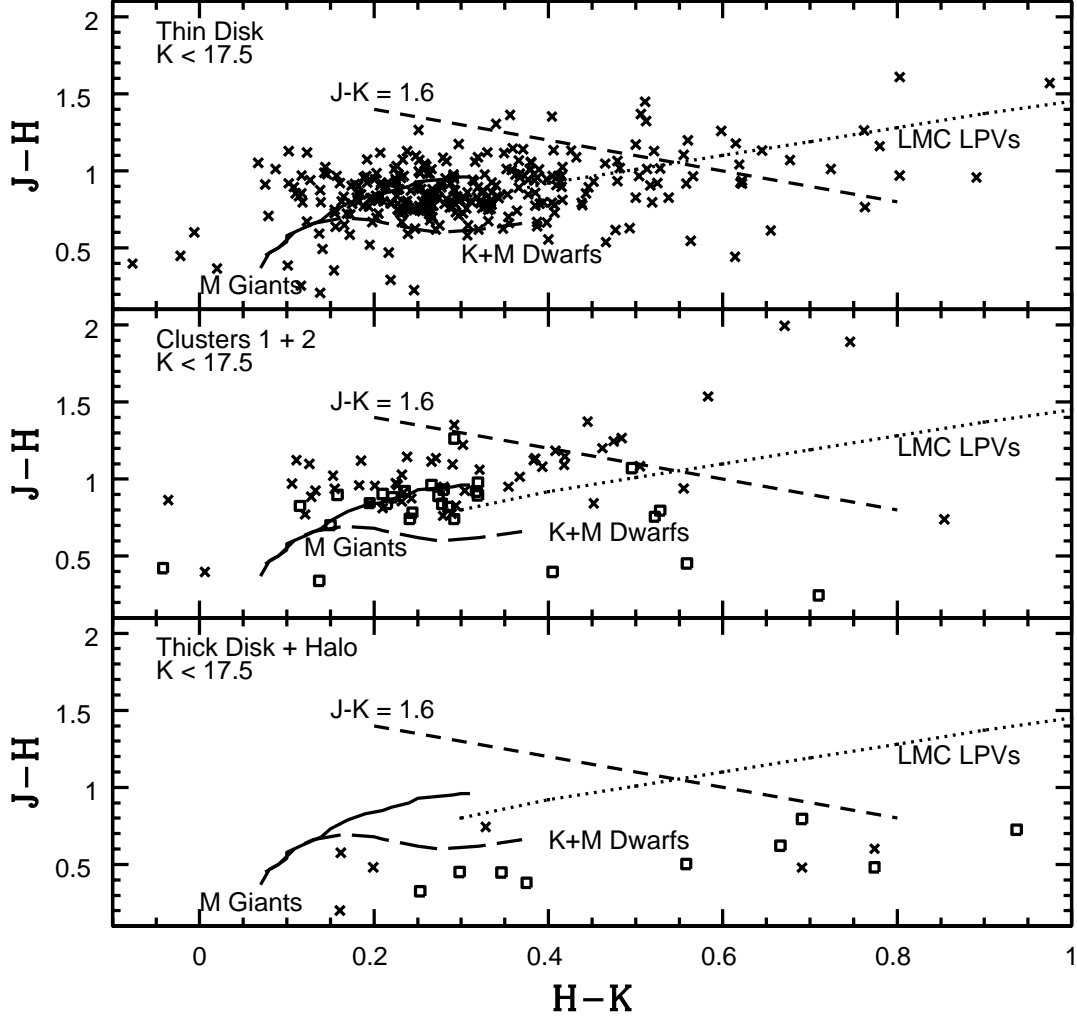


Fig. 7.— The  $(H - K, J - H)$  TCD of stars with  $K < 17.5$  in the thin disk field (top panel), Clusters 1 and 2 (middle panel), and the thick disk and halo (lower panel). Stars in the thin disk field, Cluster 1, and the thick disk are plotted as crosses, while stars in Cluster 2 and the halo are shown as open squares. The solid line is the sequence for solar neighborhood M giants from Bessell & Brett (1988), while the dotted line is the locus of LMC LPVs from Hughes & Wood (1990) and the long dashed line is the locus of K and M dwarfs from Bessell & Brett (1988). The short dashed line indicates  $J - K = 1.6$ ; Hughes & Wood (1990) find that LPVs in the LMC with  $J - K < 1.6$  tend to be M giants, while those with  $J - K > 1.6$  tend to be C stars.

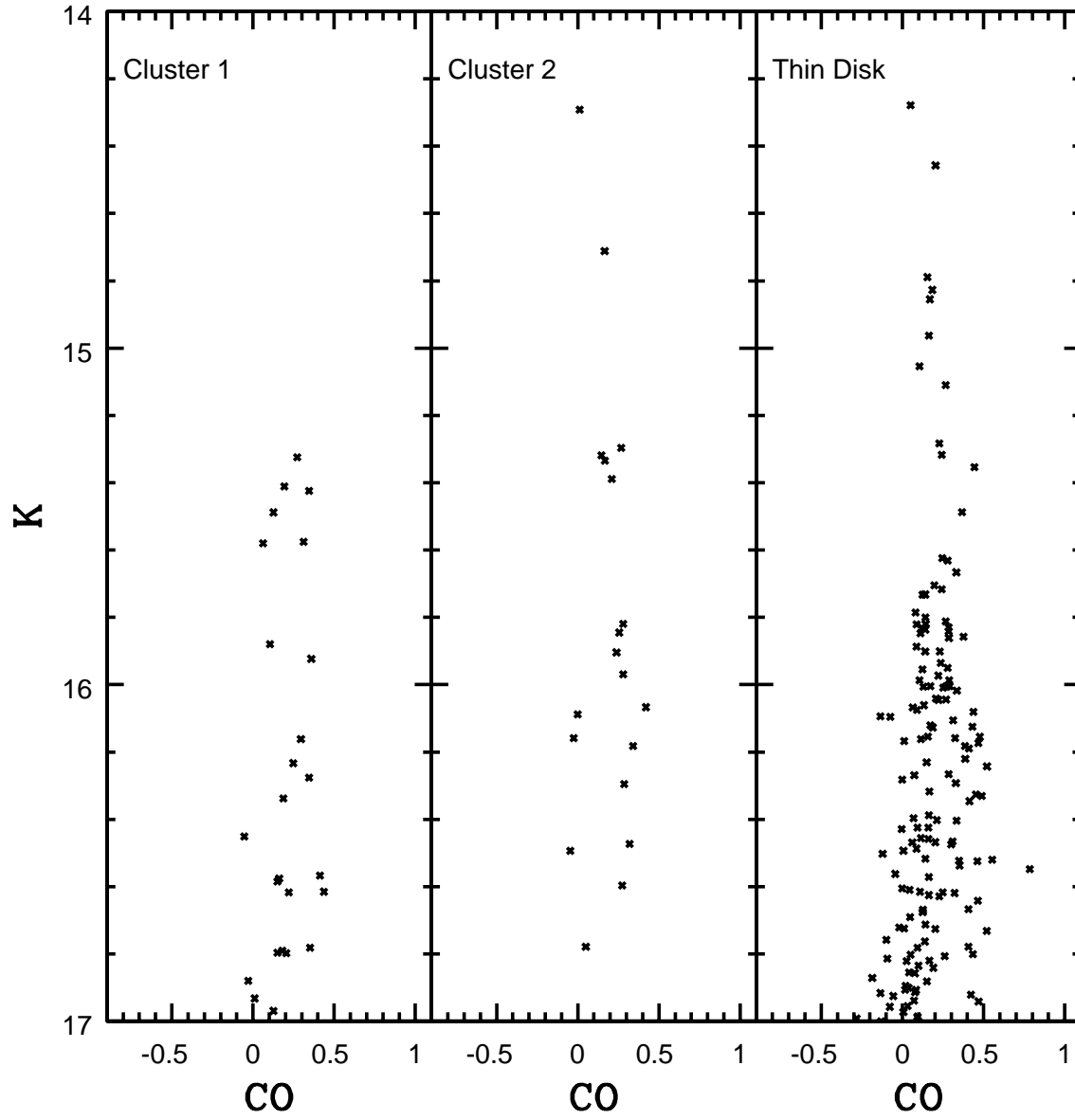


Fig. 8.— The  $(K, CO)$  CMDs of Cluster 1, Cluster 2, and the thin disk field. The vertical sequences on the CMDs are dominated by RSGs and AGB stars. Note that the brightest star in Cluster 2 and the thin disk field has a very weak CO index when compared with other stars, suggesting that it is a foreground object.

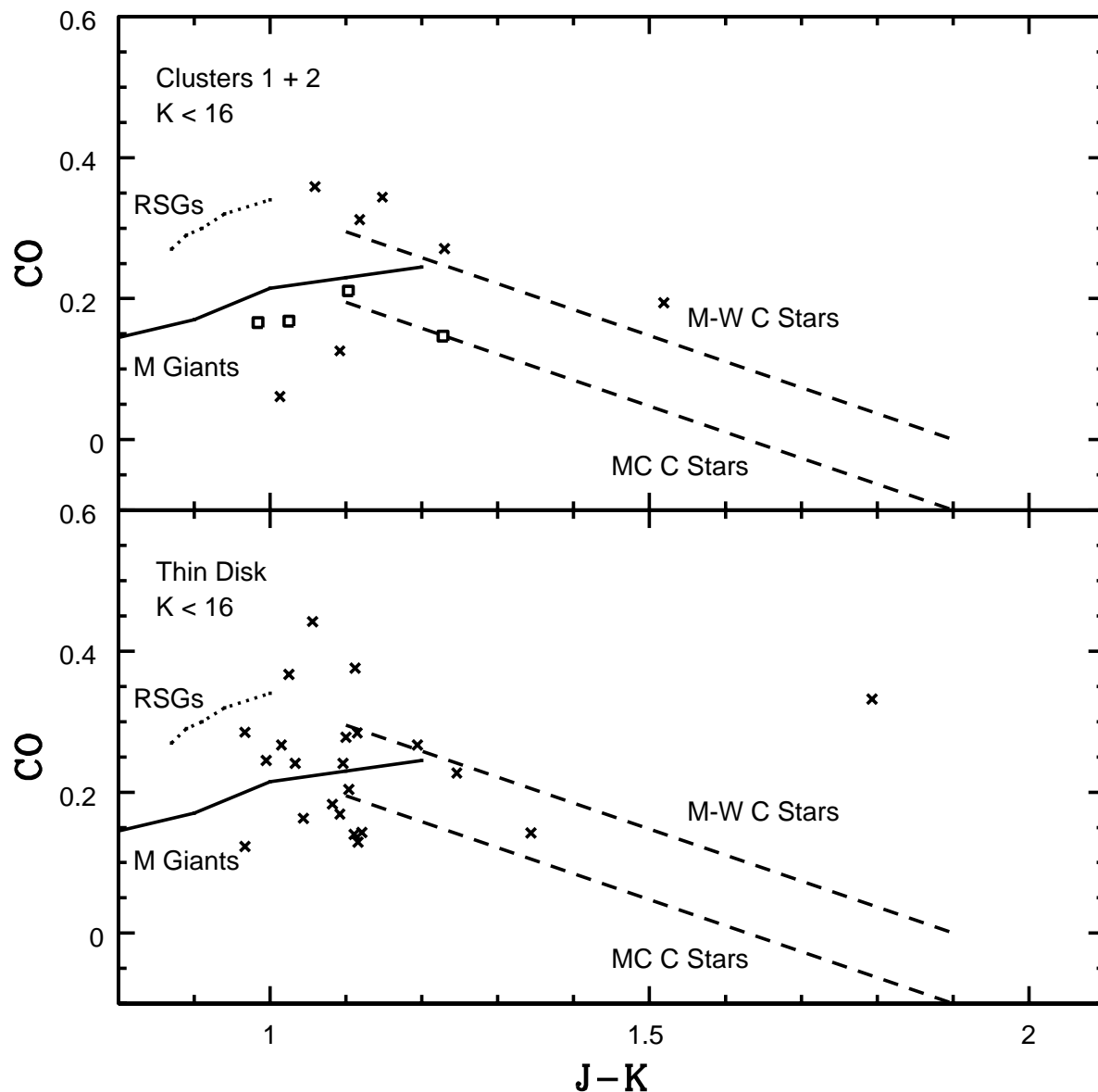


Fig. 9.— The  $(CO, J - K)$  TCD for stars with  $K < 16$  in Clusters 1 and 2 and the thin disk field. Stars in Cluster 1 and the thin disk field are plotted as crosses, while stars in Cluster 2 are shown as open squares. The solid line shows the locus of Galactic M giants from Frogel et al. (1978), while the dotted line shows the sequence for LMC RSGs from Elias, Frogel, & Humphries (1985). The dashed lines show the C star sequences for the Magellanic Clouds and the Milky-Way from Figures 3 and 4 of Cohen et al. (1980).

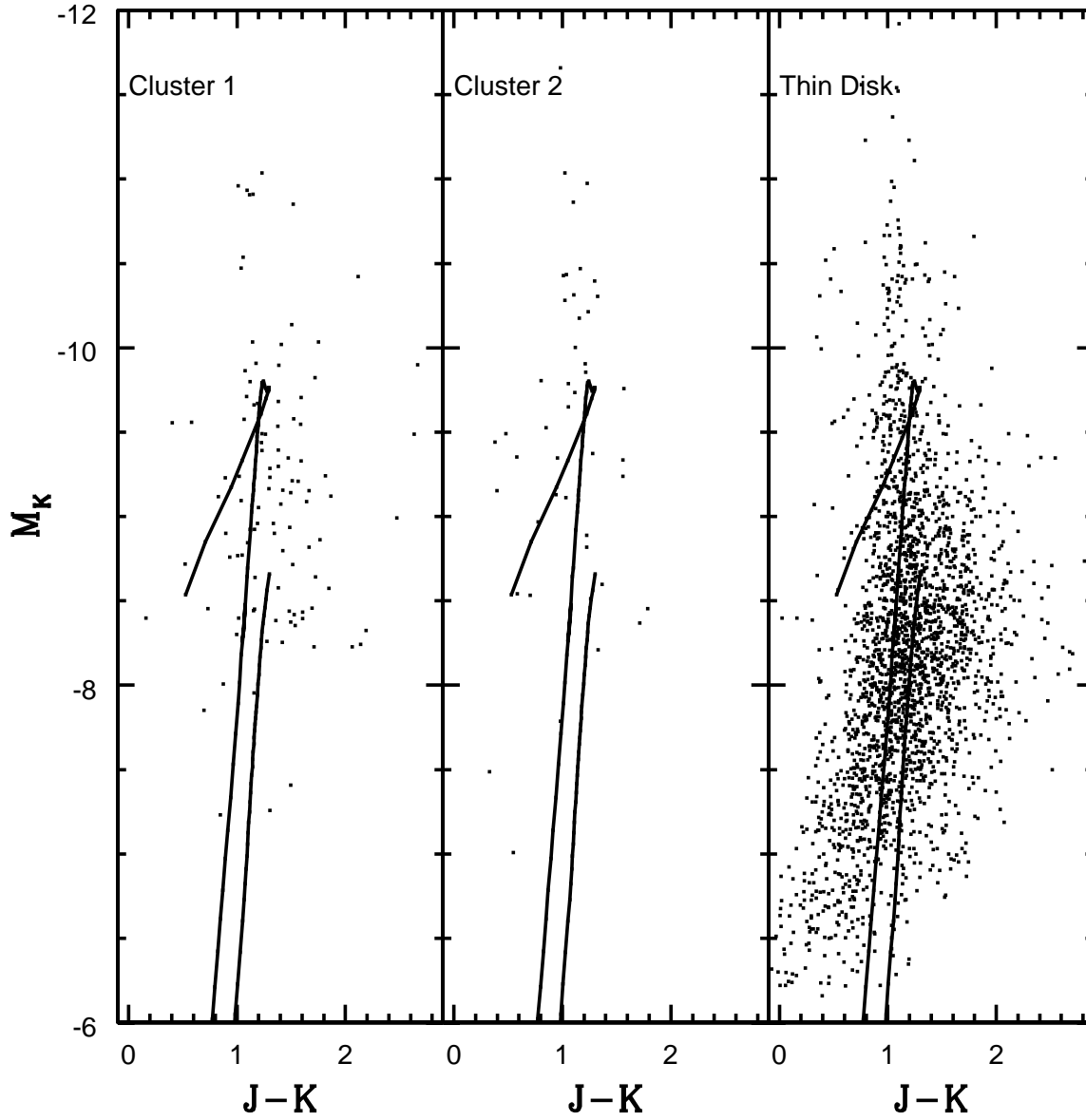


Fig. 10.— The  $(M_K, J - K)$  CMD of Clusters 1 and 2 and the thin disk. A distance modulus of 26.5 has been assumed, based on the  $i'$  brightness of the RGB-tip measured from the GMOS data. The solid lines are  $Z = 0.008$  isochrones from Girardi et al. (2002) with  $\log(t_{yr}) = 8.15$  and 9.0.

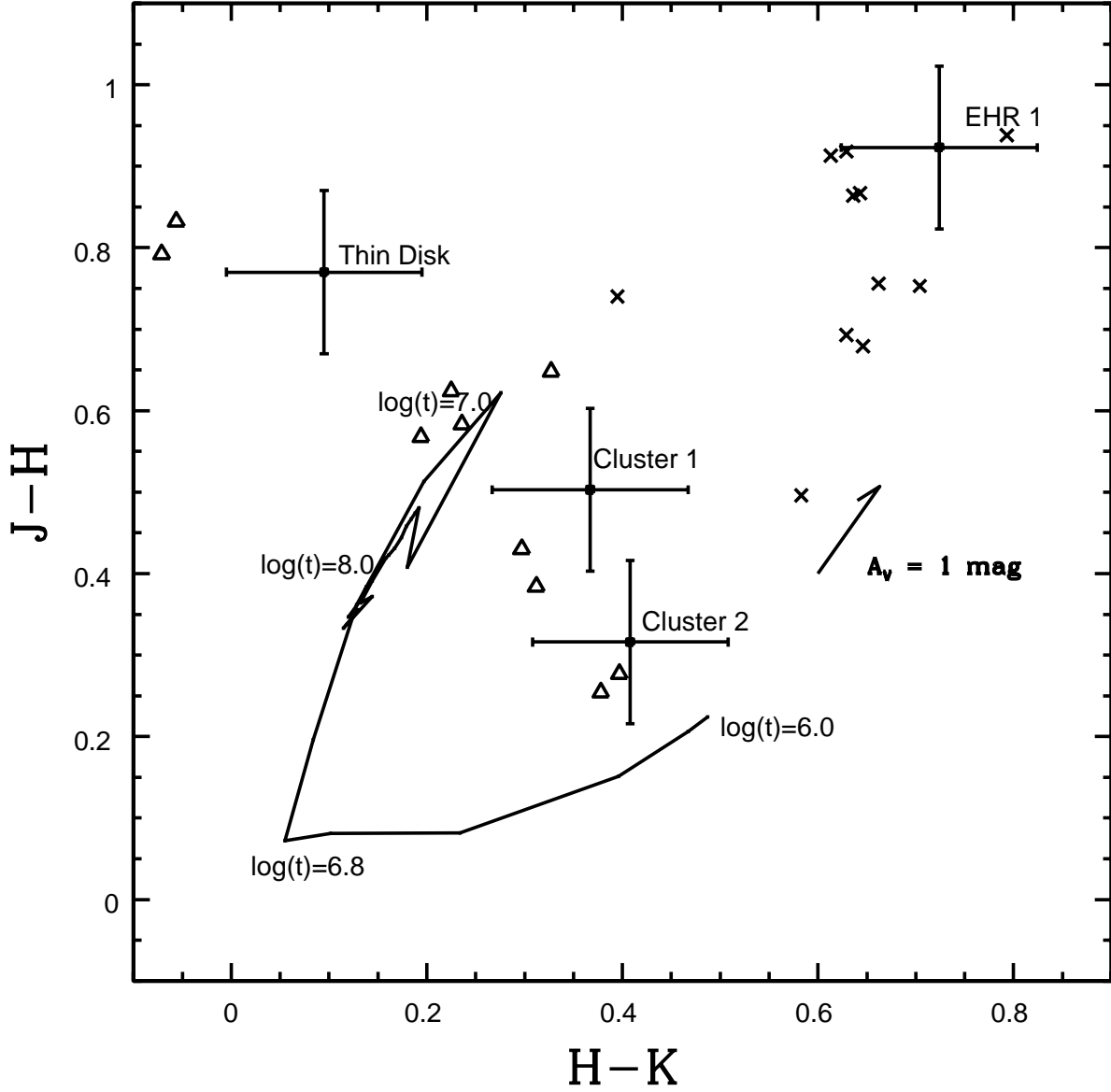


Fig. 11.— The  $(J - H, H - K)$  TCD, showing the locations of Clusters 1 and 2, the thin disk near Cluster 1, and the extraplanar HII region EHR 1. The solid line shows the locus of  $Z=0.004$  models from Leither et al. (1999) with  $\alpha = 2.35$ , and masses between 1 and 100  $M_{\odot}$ . Various ages along the sequence are indicated. The crosses are young clusters near the center of the star-forming galaxy NGC 3077 from Davidge (2004), while the open triangles are SB(s)m galaxies in the 2MASS Large Galaxy Atlas (Jarrett et al. 2003); the colors of the latter objects were computed from their total  $J, H$ , and  $K$  brightnesses. The reddening vector has a length that corresponds to  $A_V = 1$  magnitude.

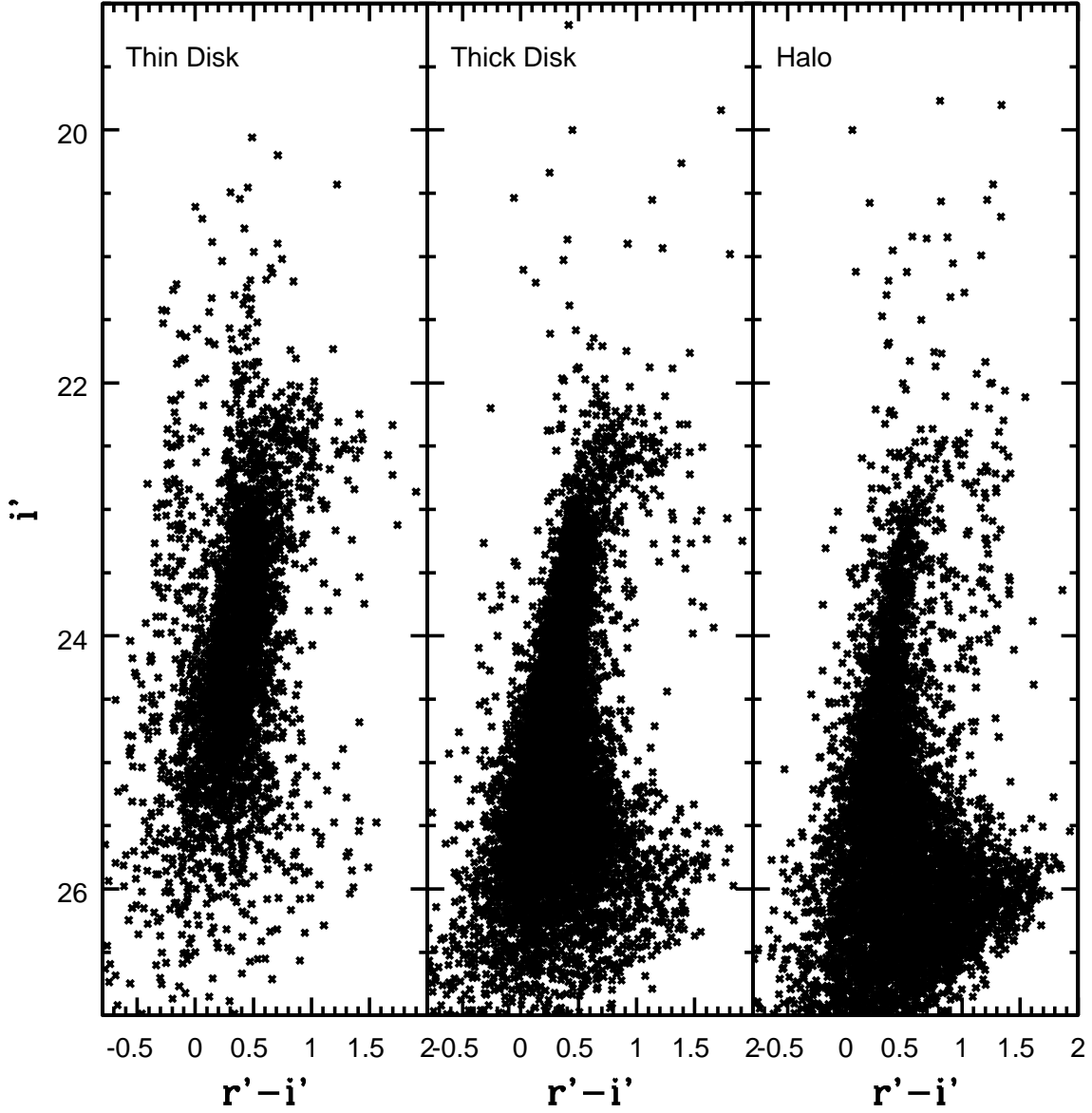


Fig. 12.— The  $(i', r' - i')$  CMDs of the thin disk, thick disk, and halo portions of the GMOS NGC 55 field.

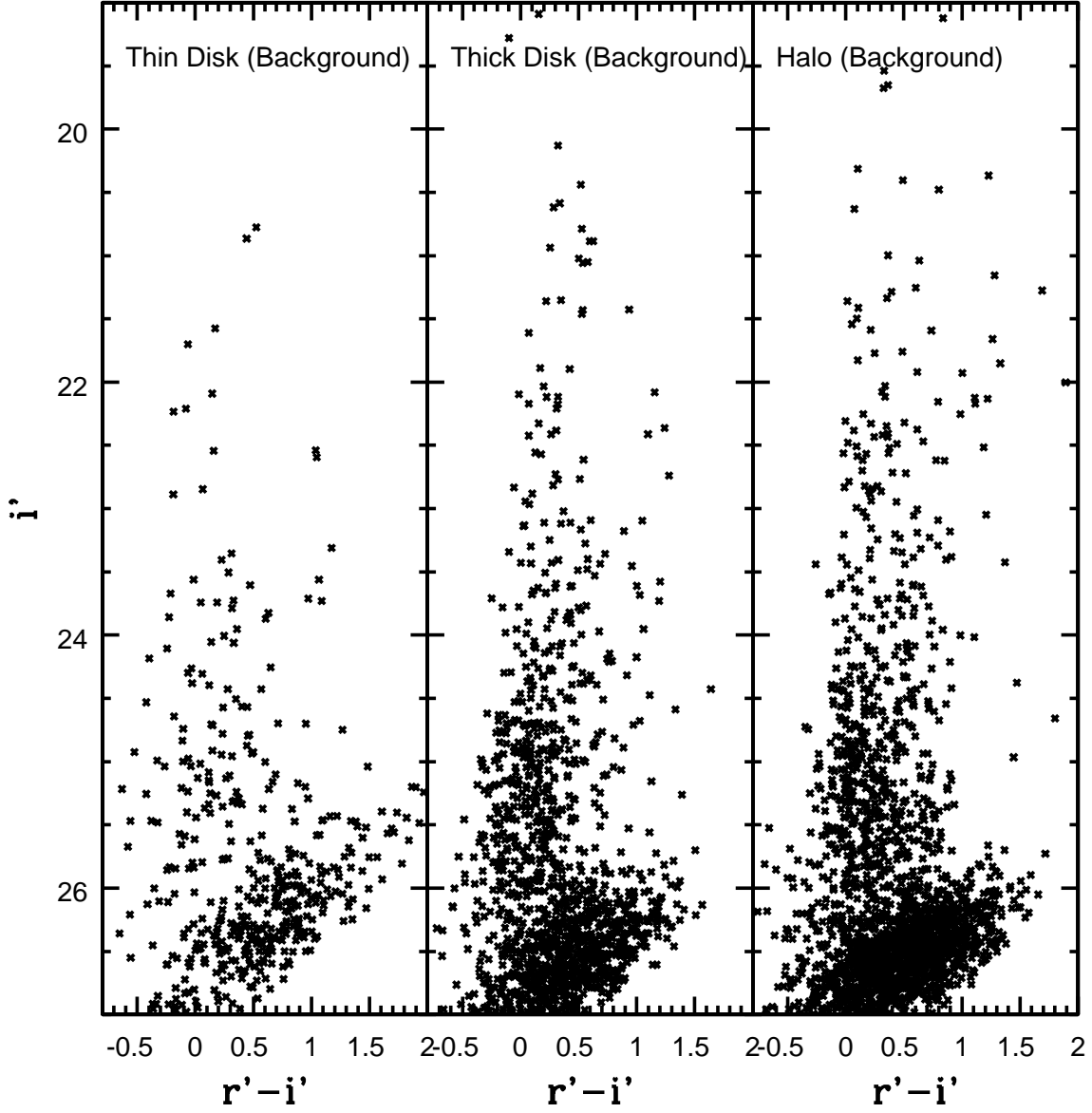


Fig. 13.— The  $(i', r' - i')$  CMDs of areas in the GMOS control field that correspond to the thin disk, thick disk, and halo regions defined in NGC 55.

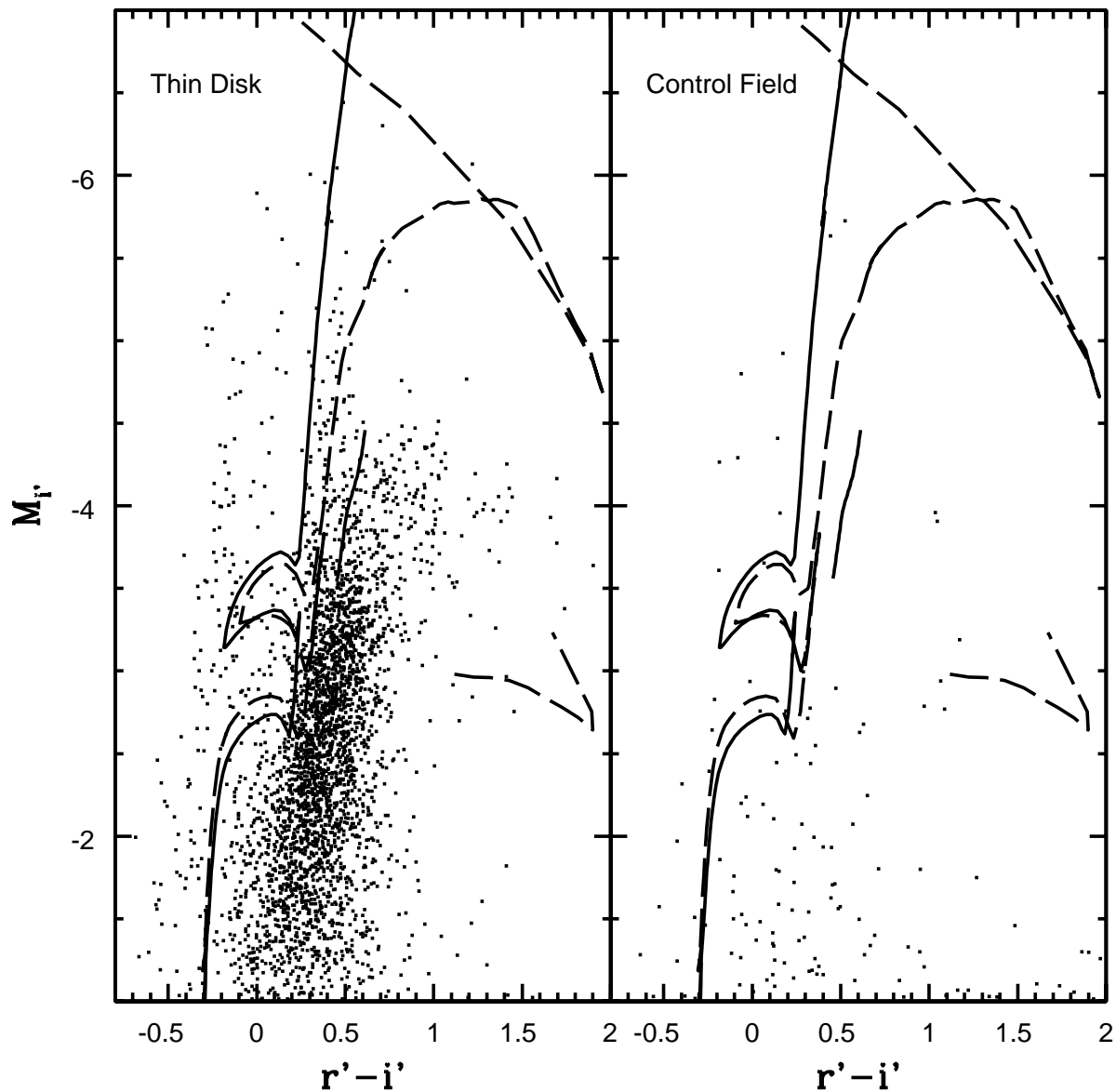


Fig. 14.— The  $(M_{i'}, r' - i')$  CMDs of the thin disk and the corresponding portion of the control field. A distance modulus of  $\mu_0 = 26.5$  is assumed, based on the  $i'$  brightness of the RGB-tip (§4.2). The solid lines are  $Z=0.008$  isochrones with  $\log(t) = 8.15$  and  $10.0$  from Girardi et al. (2002), which were transformed into the SDSS filter system using relations from Fukugita et al. (1996). The dashed lines show isochrones with the same ages, but with  $Z=0.001$ . The  $\log(t)=10$  isochrones only include the AGB.

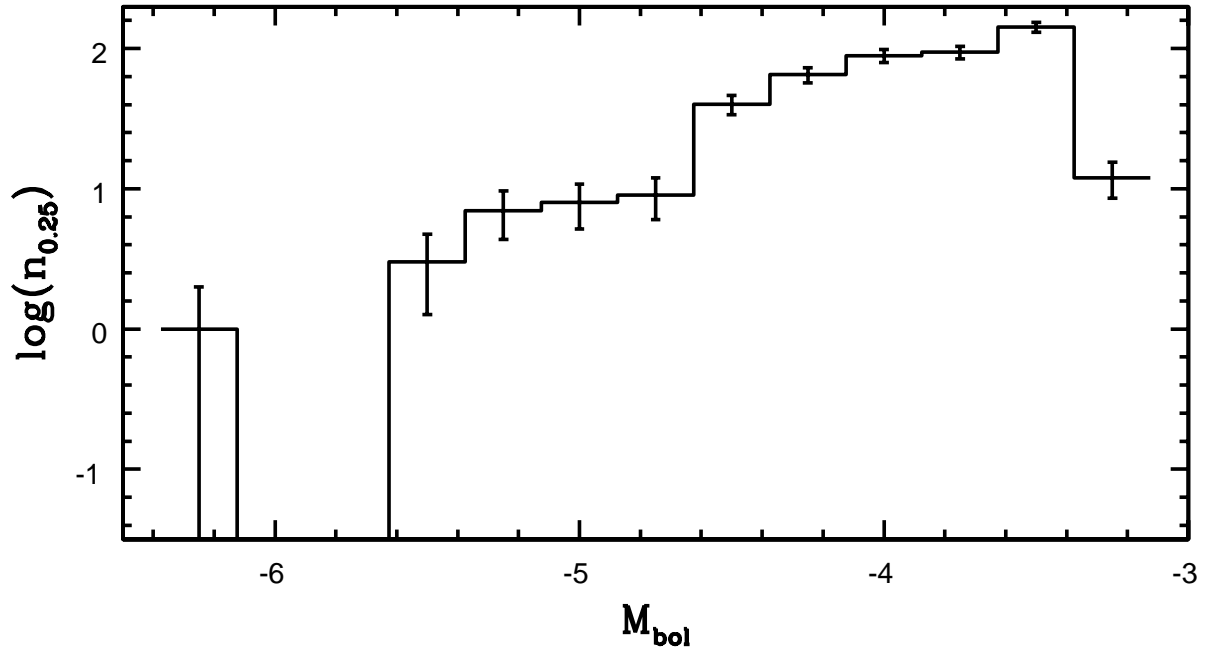


Fig. 15.— The bolometric LF of AGB stars in the thin disk, as computed from the GMOS data using the procedures described in the text. A distance modulus of 26.5 has been assumed, based on the  $i'$  brightness of the RGB-tip (§4.2).  $N_{0.25}$  is the number of stars per 0.25 mag interval in  $M_{bol}$ . Note the break in the LF near  $M_{bol} = -4.6$ . The error bars show counting statistics.

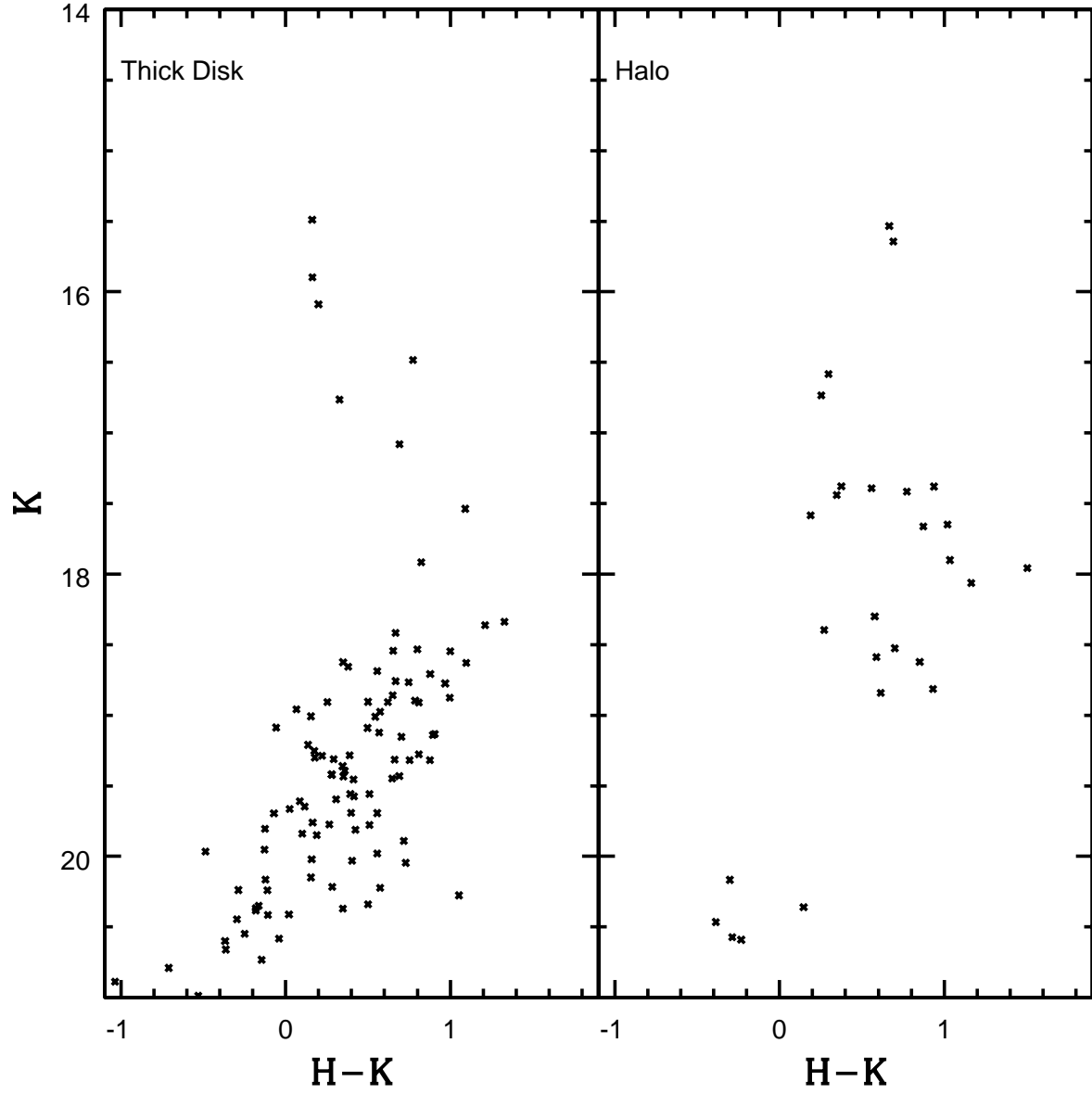


Fig. 16.— The  $(K, H - K)$  CMDs of the thick disk and halo portions of the CFHTIR strip. It is shown in Figure 7 that the bright stars in these CMDs have SEDs that differ from those of evolved stars, and hence are likely not at the distance of NGC 55.

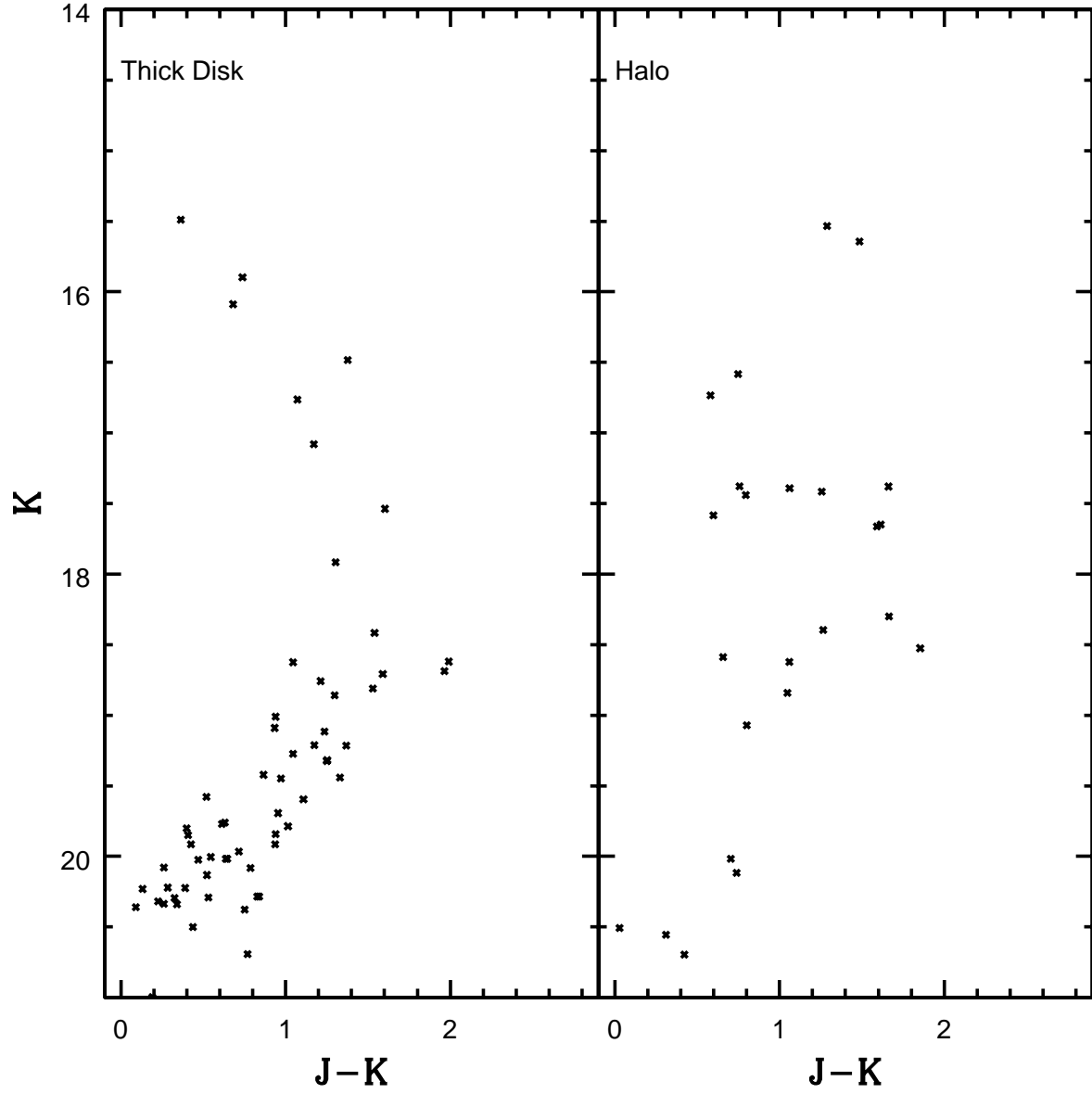


Fig. 17.— The  $(K, J - K)$  CMDs of the thick disk and halo portions of the CFHTIR strip. It is shown in Figure 7 that the bright stars in these CMDs have SEDs that differ from those of evolved stars, and hence are likely not at the distance of NGC 55.

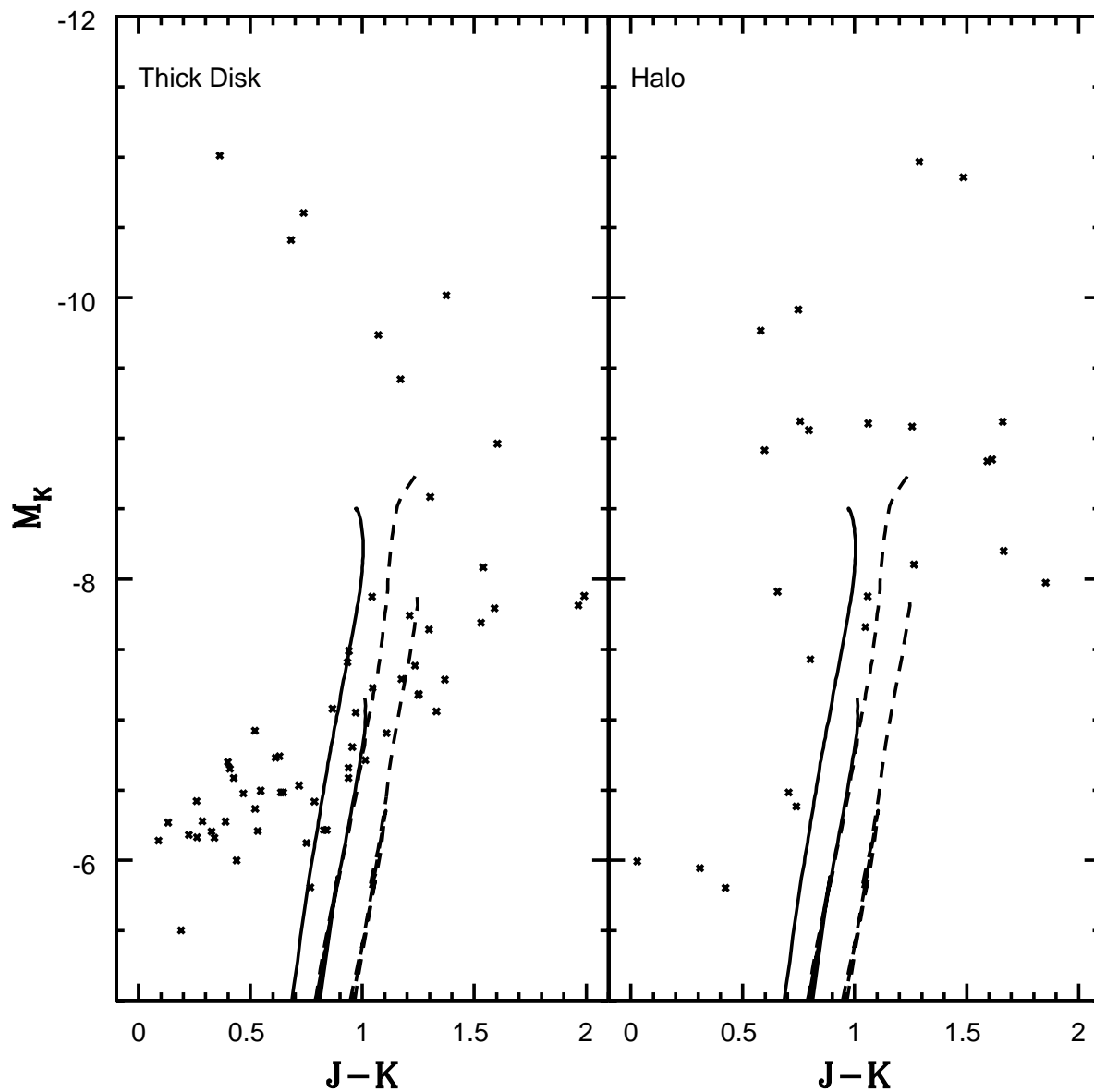


Fig. 18.— The  $(M_K, J - K)$  CMD of the thick disk and halo portion of the CFHTIR strip. A distance modulus of 26.5 has been assumed, based on the  $i'$  brightness of the RGB-tip (Section 4.2). The solid lines are  $Z = 0.001$  isochrones from Girardi et al. (2002) with  $\log(t_{yr}) = 9.0$  and  $10.0$ , while the dashed lines are  $Z = 0.004$  isochrones with the same ages.

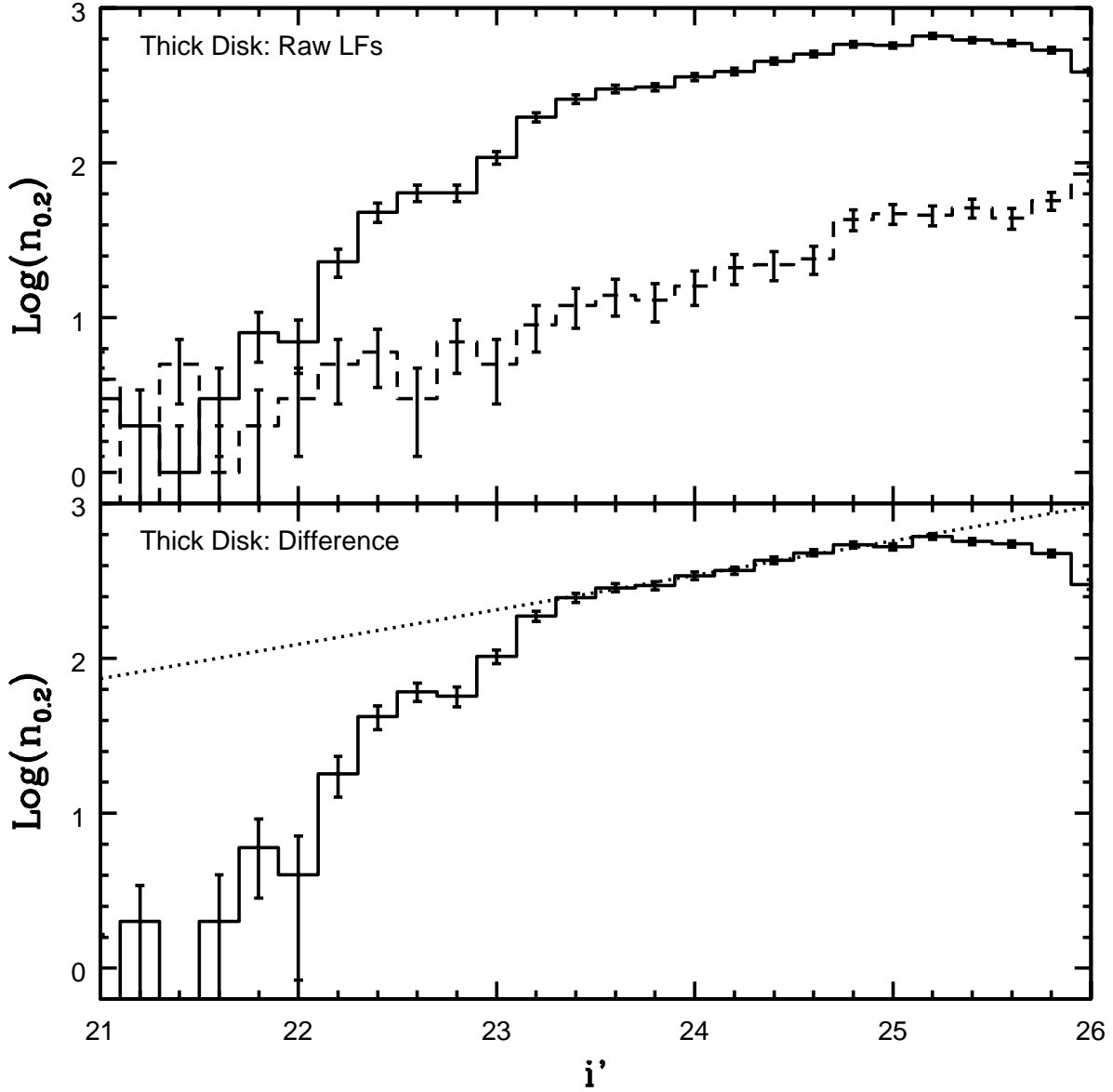


Fig. 19.— The top panel shows the  $i'$  LF of sources in the thick disk portion of the NGC 55 GMOS field (solid line) and the corresponding area of the control field (dashed line).  $n_{0.2}$  is the number of stars per 0.2 magnitude interval in  $i'$  with  $r' - i'$  between  $-0.5$  and  $1.5$ . The error bars show uncertainties due to Poisson statistics. The lower panel shows the NGC 55 LF after subtracting the control field LF. The dotted line is a power-law with an exponent  $x = 0.22 \pm 0.01$ , which was computed from the entries in the lower panel with  $i'$  between 23.5 and 25.0. Note that the LF departs significantly from the fitted power-law near  $i' = 23.1$ , and this is adopted as the brightness of the RGB-tip.

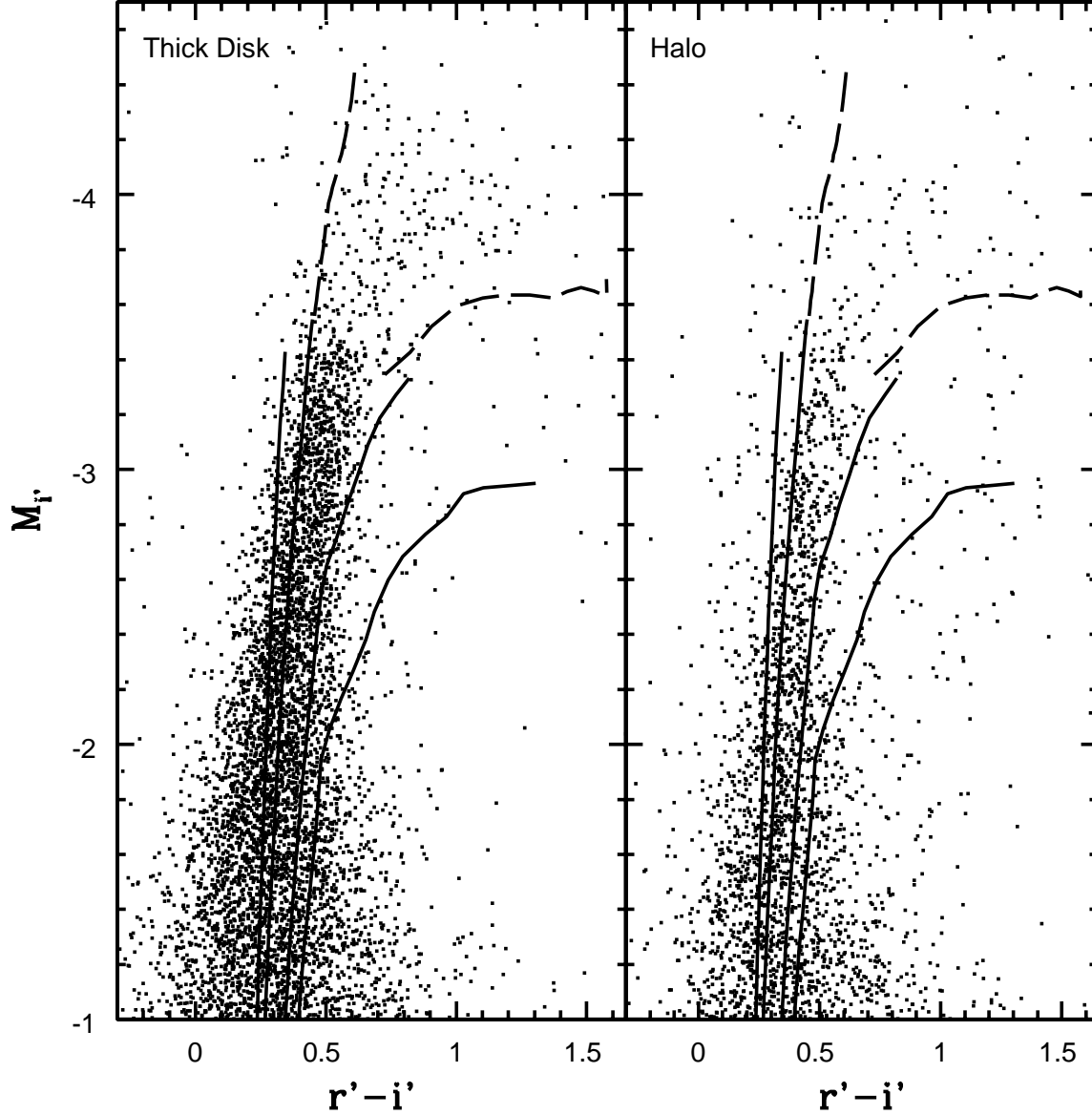


Fig. 20.— The  $(M_{r'}, r' - i')$  CMD of the thick disk and halo of NGC 55, assuming a distance modulus of 26.5 based on the  $i'$  brightness of the RGB-tip. The solid lines are RGB isochrones from Girardi et al. (2002) with  $\log(t_{yr})=10$  and  $Z = 0.0001, 0.001, 0.004$  and  $0.008$ . These isochrones were transformed into the SDSS filter system using relations from Fukugita et al. (1996). The dashed lines show the AGB extensions of the  $Z=0.001$  and  $Z=0.004$  isochrones. Note that the majority of RGB stars have a metallicity between  $Z=0.001$  and  $0.004$ , and that the brightest AGB stars have an age  $\log(t_{yr}) = 10 \pm 0.1$  dex (see text).